

CHALMERS



A Methodology for Identification of Magic Formula Tire Model Parameters from In-Vehicle Measurements

Master's Thesis in Automotive Engineering

AXEL JONSON & ERIC OLSSON

Department of Applied Mechanics
Vehicle Engineering and Autonomous Systems
Vehicle Dynamics
CHALMERS UNIVERSITY OF TECHNOLOGY
Gothenburg, Sweden 2016
Master's Thesis 2016:60

Master's Thesis in Automotive Engineering

A Methodology for Identification of Magic
Formula Tire Model Parameters from In-Vehicle
Measurements

AXEL JONSON & ERIC OLSSON

Department of Applied Mechanics
Vehicle Engineering and Autonomous Systems
CHALMERS UNIVERSITY OF TECHNOLOGY
Gothenburg, Sweden 2016

A Methodology for Identification of Magic Formula Tire Model Parameters from
In-Vehicle Measurements
AXEL JONSON & ERIC OLSSON

© AXEL JONSON & ERIC OLSSON, 2016

Master's Thesis 2016:60
ISSN 1652-8557
Department of Applied Mechanics
Vehicle Engineering and Autonomous Systems
Chalmers University of Technology
SE-412 96 Gothenburg
Sweden
Telephone: + 46 (0)31-772 1000

Cover:
Volvo V40 CC test vehicle performing maneuver to measure linear range tire data.

Department of Applied Mechanics Gothenburg, Sweden 2016

A Methodology for Identification of Magic Formula Tire Model Parameters from
In-Vehicle Measurements
Master's Thesis in Automotive Engineering
AXEL JONSON & ERIC OLSSON
Department of Applied Mechanics
Vehicle Engineering and Autonomous Systems
Chalmers University of Technology

Abstract

Accurate tire modeling is of key importance to the development of modern vehicles. Traditional Flat-Trac testing of tires is expensive and time consuming. In order to increase the efficiency of the vehicle development process, a new method for identifying Magic Formula tire model parameters has been investigated. By driving specific maneuvers with a vehicle instrumented with sensors to measure wheel forces and angles, tire model parameters can be estimated by use of a global optimization algorithm. Full vehicle simulations were made in order to identify the test procedures necessary to provide a representative range of data for a tire. A tire model parameter fitting tool was developed and validated with Flat-Trac datasets. Physical testing was carried out to reproduce the simulated driving maneuvers on a car equipped with wheel force transducers, an inertial measurement device, and a high-speed camera system to measure wheel angles and displacements. Results of estimating the pure slip lateral tire model parameters from the in-vehicle measurements shows good correlation to the original tire model. Furthermore, the tire model parameters identified by this method more accurately represent the behavior of the tire on the test vehicle, without the need to modify scaling parameters. This indicates that this newly proposed method can produce accurate tire model parameters that require less tuning of scaling parameters to accurately represent vehicle behavior.

Keywords: Magic formula, Pacejka, Pac2002, tire modeling, vehicle modeling, in-vehicle measurements, tire measurements, lateral force, slip angle, pure slip, steady-state.

Acknowledgments

We would like to thank everyone who helped us throughout this thesis work. Thank you Stefan Karlsson and Egbert Bakker at Volvo Cars for your support with technical knowledge and guidance. Thank you, Edward Gruia, also at Volvo Cars, for all the help with the measurement equipment and testing, without which there would be no results. Also a big thank you to Anton Albinsson and our examiner Mathias Lidberg at Chalmers University of Technology for your technical consultation and support.

Axel Jonson & Eric Olsson, Gothenburg, July 11, 2016.

Contents

1	Introduction	1
1.1	Tire Measurement	1
1.1.1	TIME Project	2
1.2	Online Tire Force Estimation	3
1.3	Hällered Proving Ground	4
1.4	Scope	5
2	Theoretical Background	7
2.1	Tire Behavior	7
3	Vehicle & Tire Modeling	12
3.1	Vehicle Modeling	12
3.1.1	Load transfer	14
3.1.2	Wheel orientation	15
3.2	Magic Formula Tire Model	17
3.2.1	Slip angles	19
4	Using the Vehicle as a Tire Testing Machine	21
4.1	Limitations of In-vehicle Measurements	21
4.1.1	Load transfer	23
4.1.2	Wheel orientation	24
4.1.3	Slip angles	24
4.2	Simulations	25
4.3	Design of Vehicle Maneuvers & Procedures	26
4.3.1	Required Data range	26
4.3.2	Linear Maneuver	26
4.3.3	Non-Linear maneuver	29
4.4	Vehicle Preparation	31
4.4.1	Front Camber Adjustment	31
4.4.2	Rear Camber Adjustment	34

4.5	Instrumentation	35
4.5.1	Data Acquisition System	36
4.5.2	Wheel Force Transducers	36
4.5.3	Inertial Measurement Unit	38
4.5.4	Optical Wheel Measurement System	39
4.5.5	Wheel Travel Transducers	40
4.5.6	CAN Bus	40
4.6	In-Vehicle Measurements	40
4.6.1	Test Schedule	40
4.6.2	Tire Temperatures	41
4.6.3	Linear Maneuver	42
4.6.4	Non-Linear Maneuver	46
5	Tire Model Parameter Identification Method	50
5.1	Post-Processing of Measurement Data	50
5.2	Method	52
5.3	Fitting Requirements	54
5.4	Non-Linear Constraints	54
5.5	Parameter Bounds	54
5.6	Genetic Algorithm	55
5.7	Validation of Fitting Tool	55
6	Identification of Magic Formula Tire Model Parameters	59
6.1	From Lateral Force with Gaussian Noise	59
6.2	From Simulation Data	60
6.3	From Measurement Data	62
7	Discussion	70
7.1	Testing procedure	70
7.1.1	Maneuvers	70
7.2	Magic Formula Parameter Fitting Method	70
7.3	Tire Phenomena	71
7.4	Limitations	73
7.5	Advantages	74
8	Conclusion	75
	Bibliography	77
A	Appendix	78
A.1	Notations	78
A.1.1	Vehicle Definitions	78
A.2	Magic Formula Equations	79
A.3	Validation of Measured Data	82

A.4 Fitting Tool	85
A.4.1 Graphical User Interface	85

1

Introduction

The automotive industry is a very competitive market, and development is fast. Cost effective solutions with short project lead times are necessary to survive in today's global competition. In vehicle dynamics this means that more development is being done virtually, reducing the need for costly prototype vehicles. Virtual development also allows for optimization which makes it possible to converge on more effective and mature solutions.

A vehicle's only contact with the ground is through its tire contact patches. All forces between the car and the road are generated and transmitted through them. Tire characteristics can vary greatly between different tires, and are dependent on design properties such as size, rubber compound, construction of the tire carcass, and tread pattern, but also on ambient conditions such as road type, temperature, and humidity levels. It is easy to understand that accurate tire modeling is very complicated, but also necessary for satisfactory vehicle dynamics simulations. Accurate tire models are of course necessary for predicting the vehicle path and behavior, but they are also needed for being able to correctly specify and develop different suspension subsystems, such as suspension bushings.

1.1 Tire Measurement

Traditional testing of tire behavior is conducted on a machine that can independently manipulate normal load, road speed, slip quantities, inclination angle, and tire pressure. The forces and moments on the tire are then measured and recorded. These machines are usually extremely stiff so that errors in the measurements due to deflections are reduced. Some of these machines have a belted surface, and others use a cylindrical roller to represent the road. The MTS Flat-Trac Tire Testing System is shown in Figure 1.1.

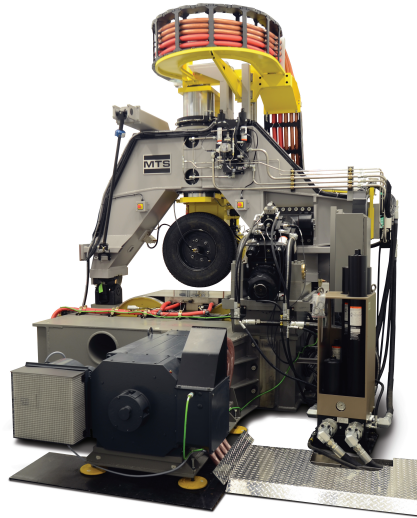


Figure 1.1: MTS Flat-Trac[®] CT Plus Tire Test System. Photo courtesy of MTS Systems Corporation © 2014

Because these machines can independently change the different input variables to the Magic Tire Formula, they are therefore extremely useful for collecting data over a wide range of operating conditions. Also since these machines reside in a lab environment, it is easy to add other sensors to monitor variables such as temperature and humidity to ensure consistent results between tests. Some of these machines also have the ability to conduct testing on wet and low- μ surfaces. However, because of the high precision and functionality of these machines, they are expensive to purchase and therefore expensive to hire, so tire testing can be very expensive for vehicle and tire manufacturers. These machines also cannot collect data on actual road surfaces, of special interest being the specific surfaces found on different proving grounds. With a tire model created for a specific road surface, simulation models can be validated against physical vehicles more accurately. Several types and manufacturers of these machines exist, which introduces errors when comparing data that was measured using different machines. Because of the variance between machines, test procedures, and measurement equipment, research has been done with the aim to create more robust tire testing procedures.

1.1.1 TIME Project

In 1999 a joint effort between tire manufacturers and vehicle designers was made to create a tire testing procedure with the goal of increasing the accuracy and precision of the tire data (Oosten, 1999 [2]). This project investigated the results from measuring tires on several different tire measurement machines in order to identify the magnitude of error between them. It was found that by using standard slip angle sweep tests measured over several constant normal loads, typical errors between the 11 machines that tested 6 different tires resulted in up to a 63% difference in the cornering stiffness of the

tire, as seen in Table 1.1.

Tire Type	Sequence 1			Sequence 4			Sequence 5		
	Max	Min	Range	Max	Min	Range	Max	Min	Range
195/65R15	1858	1229	41 %	1756	1232	35 %	1748	1234	35 %
225/60R16	1956	1227	46 %	1928	1000	63 %	1907	1206	45 %
155/70R13	858	626	31 %	861	552	44 %	955	510	61 %
175/70R14	1055	810	26 %	1010	713	34 %	1024	736	33 %
165/70R13	1007	714	34 %	951	557	53 %	965	671	36 %
225/60R15	1776	1196	39 %	1734	1182	38 %	1748	1212	36 %

Table 1.1: Ranges between the maximum and minimum cornering stiffness [N/deg] (Oosten, 1999 [2])

In order to improve the accuracy and precision of tire testing, a new test procedure was proposed that more accurately represents a tire’s behavior on a vehicle. Instead of slip angle sweeps at constant normal load and camber angles, the new procedure reproduces the behavior of a vehicle driving around a track with a variety of corner radii and speeds. This procedure varies all the parameters simultaneously in order to represent a vehicle with load transfer and varying camber angles. The effect of this change in test procedure resulted in reducing the cornering stiffness error to 10% between different tire testing machines when the new procedure was followed.

The new method developed in this research extends the TIME project work by allowing a vehicle to be used as the tire testing machine, while driving specifically designed maneuvers to capture the tire characteristics. This is possible in part due to the fact that vehicle testing at proving grounds is becoming more and more sophisticated, with the possibility to use high accuracy measurement equipment that has previously been unrealistic for vehicle dynamics testing.

1.2 Online Tire Force Estimation

Modeling a tire requires detailed knowledge of the individual forces that are generated at the operating conditions of interest. It is therefore necessary to measure the force at the wheel, for example using wheel force transducers (Chapter 4.18), or a tire measurement rig (Chapter 1.1).

A simplified approach can be to utilize the sensors that are already built in to most new cars, using the bicycle model in Figure 1.2. It is a simple model where the tire

characteristics, suspension kinematics, and suspension compliances are lumped into a single axle characteristic. With this model, the axle forces can be calculated knowing only the vehicle inertia and accelerations, using a force and moment balance. The axle slip angles are calculated as in equation 2.3.

The force and slip angle data can then be used to parameterize any tire model of choice. Since the resulting model will incorporate the effective use of both tires, as well as the suspension characteristics, it does not allow for altering the vehicle. A change of anti-roll bar, for example, would require new data collection and an all new model parameterization.

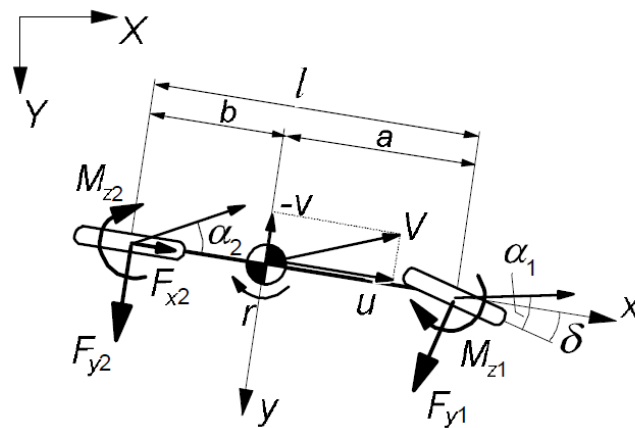


Figure 1.2: The bicycle model. A simple 2 DOF model where the tire characteristics are lumped into axle characteristic (Pacejka, 2012 [3])

1.3 Hällerred Proving Ground

Hällered Proving Ground is one of Volvo Cars' vehicle testing facilities. The tire measurement testing requires a large open smooth area with even grip levels. There are two possible areas available: the Brake and Handling Area, which is 200x40m, and the Skidpad, a paved circle with a diameter of 50m. Figure 1.3 shows an aerial photo of the facility.



Figure 1.3: Hällered Proving Ground as seen from the air. The skidpad area can be seen in the middle.

1.4 Scope

The purpose of this thesis is to develop a procedure and tools to produce a tire model that accurately represents a tire's behavior from in-vehicle measurements. The method developed in this thesis applies to the Magic Formula tire model, and may work for other empirical tire models, but does not apply to physical tire models. The limitations of this work are to investigate the case of pure lateral slip, so longitudinal and turn slip forces and moments are assumed to be zero. To reduce complexity, only steady state tire behavior is to be modeled, and all transient effects are neglected.

The magic formula does, in its original form, not take the influence of tire pressure, temperature, and ambient conditions such as surface type and condition into account. To account for this one method is to parameterize one model for each case. For example a tire could be measured and parameterized for different tire pressures or temperatures. While the method developed in this thesis might be well suitable for such methods, it is not within the scope of this thesis to research the influence of varying tire and surface parameters.

Due to the limitations in temperature dependencies, constant pressure assumption, and the omission of transient influence, a major challenge will be to find driving maneuvers that allow collection of the required range of data, all while keeping effects from excessive

1.4. SCOPE

heat build-up, tire pressure change, and transients within a tolerable level.

2

Theoretical Background

2.1 Tire Behavior

The force generated by a specific tire is dependent on a number of variables. Pacejka (2012, [3]) describes the behavior and modeling of tires meticulously. When modeling tires, the tire is considered to have three different slip components: longitudinal slip – the slip ratio, lateral slip – the slip angle, and turn slip. The contribution from turn slip is significant only at low speeds, such as parking maneuvers, and will therefore not be considered in this thesis. The independent variables in the tire force equations are therefore defined as in equation 2.1.

$$F_x = F_x(\kappa, \alpha, \gamma, F_z), F_y = F_y(\kappa, \alpha, \gamma, F_z), M_z = M_z(\kappa, \alpha, \gamma, F_z) \quad (2.1)$$

Effective radius (r_e): The tire effective radius is the actual radius of the tire. For a free rolling wheel, the longitudinal speed V_x , and the rotational speed Ω_0 gives the effective radius

$$r_e = \frac{V_x}{\Omega_0} \quad (2.2)$$

A pneumatic tire rolling straight ahead in an upright position can be considered free rolling. For the tire to generate a force it needs to generate a slip quantity.

Slip angle (α): The lateral slip (angle) is defined as the angle between the heading of the wheel and its direction of travel, as given by equation 2.3.

$$\begin{aligned} V_{sy} &= V_y \\ \tan\alpha &= \frac{V_{sy}}{|V_x|} \end{aligned} \quad (2.3)$$

2.1. TIRE BEHAVIOR

Slip ratio (κ): The slip ratio is the ratio between the rotational speed of the wheel and the longitudinal speed, as given by equation 2.4

$$\kappa = -\frac{V_x - r_e * \Omega}{V_x} = -\frac{\Omega_0 - \Omega}{\Omega_0} \quad (2.4)$$

Inclination angle (γ): The angle between the road plane's Z-axis and the wheel plane, about the wheel's X-axis.

Wheel axis system: An axis system with the origin at the intersection of the wheel plane and the wheel spin axis, shown in Figure 2.1

Tire axis system: An axis system with the origin at the intersection of the wheel plane and the contact patch, shown in Figure 2.2

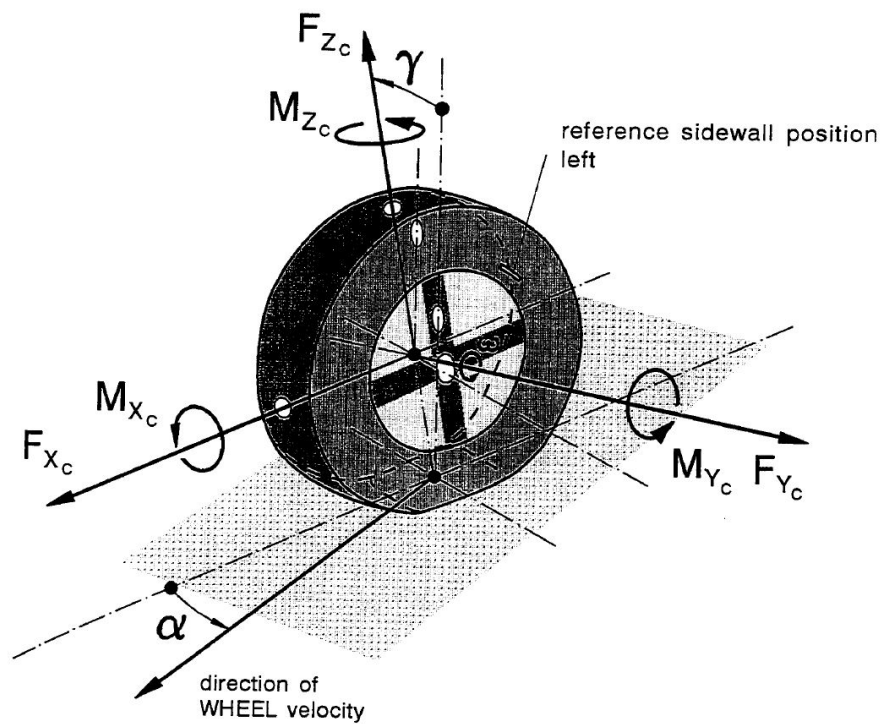


Figure 2.1: TYDEX C-Axis system. (TNO Road-Vehicles Research Institute, 1997 [4])

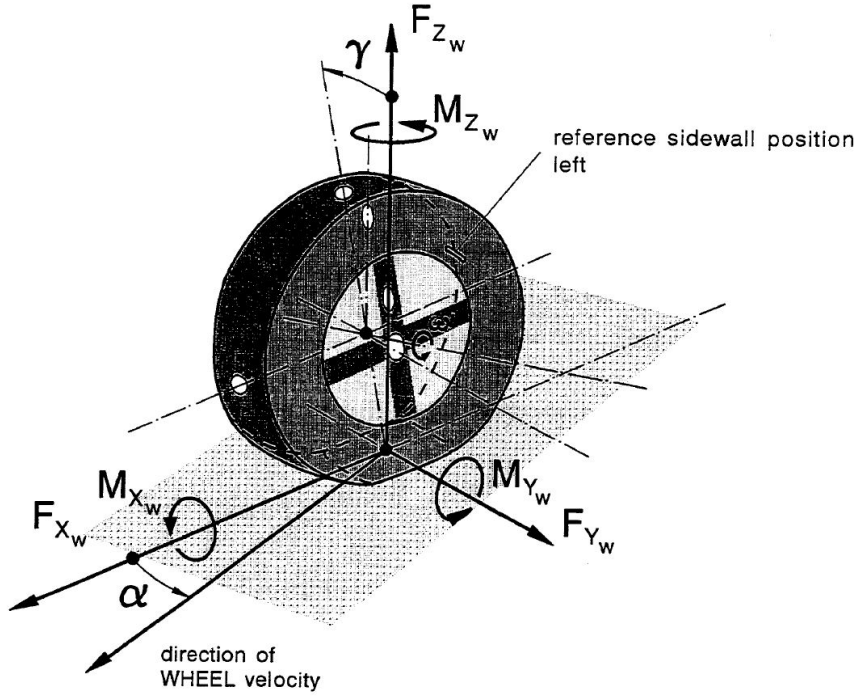


Figure 2.2: TYDEX W-Axis system. (TNO Road-Vehicles Research Institute, 1997 [4])

At low slip, the tire contact patch is not sliding on the surface. The force generated by the tire is almost linear with the slip angle. The lateral proportionality constant is referred to as the cornering stiffness ($C_{F\alpha}$), and the longitudinal constant is called the longitudinal stiffness. When the slip increases, partial sliding of the contact patch starts. The tire stiffness then decreases, and the tire starts to saturate. Figure 2.3 shows a typical tire curve for lateral force at a specific normal load and camber angle. At small slip angles the tire force is proportional to the slip angle with the cornering stiffness. Partial sliding then begins and the tire starts to saturate, and reaches its maximum friction.

When using the tire both longitudinally and laterally, i.e. in combined slip, both the longitudinal and the lateral force will decrease. The tire has a specific friction coefficient to use in any direction. This introduces the concept of a friction circle, where the total force exerted by the tire is governed by equation 2.5. Figure 2.4 shows typical tire curves during combined lateral and braking events. The concept of a friction circle is however a simplification, as in reality the friction circle is often more like an oval.

$$F_{tot} = \sqrt{F_x^2 + F_y^2} \quad (2.5)$$

Aligning moment is the tire's moment about its z-axis, and is to a large extent the source of the moment that the driver has to counteract through the steering wheel. It can be considered as built up by two different quantities (equation 2.6). Since the lateral force

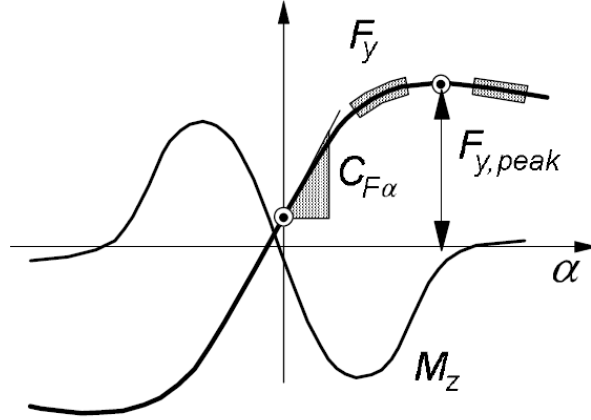


Figure 2.3: Illustration of a generic tire curve for lateral slip. (Pacejka, 2012 [3])

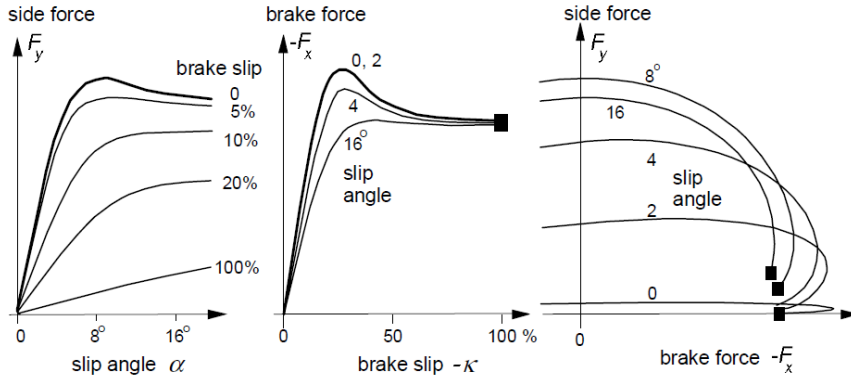


Figure 2.4: Illustration of typical tire curves for longitudinal, lateral, and combined slip. (Pacejka, 2012 [3])

application point is not coinciding with the YZ center plane of the tire, the offset gives raise to a moment. This offset is called the pneumatic trail (t). Asymmetries in the tire can also result in a moment, called the residual moment (M_{res}). A generic curve for the aligning moment can be seen in Figure 2.3. The decrease seen in aligning moment at high slip angles is due to that the length of the pneumatic trail decreases as the slip angle increases.

$$M_z = -t * F_y + M_{res} \tag{2.6}$$

In Figure 2.3 it is visible that the tire lateral force is nonzero when the slip angle is zero. This behavior is called shifts, and it is due to non-symmetries in the tire. The asymmetries causes the tire to deform in two different ways, causing conicity and ply-steer. In Figure 2.5 these concepts are explained.

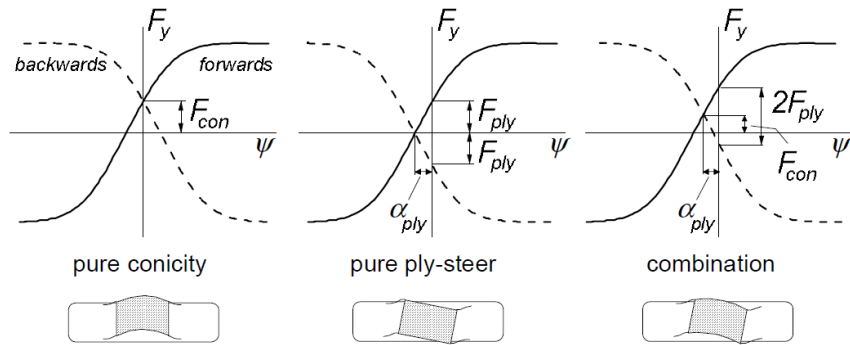


Figure 2.5: Reasons for shifts, due to asymmetries in the tire. (Pacejka, 2012 [3])

The camber angle influences the cornering stiffness as well as the peak force that the tire can generate. Typically when turning, an outer wheel with negative camber will generate more lateral force due to its favorable deformation of the contact patch. By the same logic, an outer wheel with a positive camber angle will generate less lateral force. This is true to a certain limit where the force starts decreasing again. Since camber angles also introduces asymmetry to the tire, it is a significant source to the shifts of the tire curves that can be seen in Figure 2.3. The residual aligning moment is also heavily influence by camber.

3

Vehicle & Tire Modeling

3.1 Vehicle Modeling

In order to identify the individual tire characteristics, rather than the effective axle characteristics, a high fidelity vehicle model which represents the forces, moments and displacements of each individual wheel is necessary. To achieve that in modeling, a two-track model with the kinematics and compliance (K&C) behavior of each wheel has been used. Accurate modeling of the suspension, in terms of springs, dampers, anti-roll bars, and geometries, is necessary to achieve realistic load transfer. An accurate tire model that is compatible with the high fidelity vehicle model is of course also necessary. Figure 3.1 shows a schematic of such a model. In this thesis the vehicle dynamics modeling and simulation software VI-CarRealTime was used. The following chapter aims to explain the basic theory of the model used in VI-CRT.

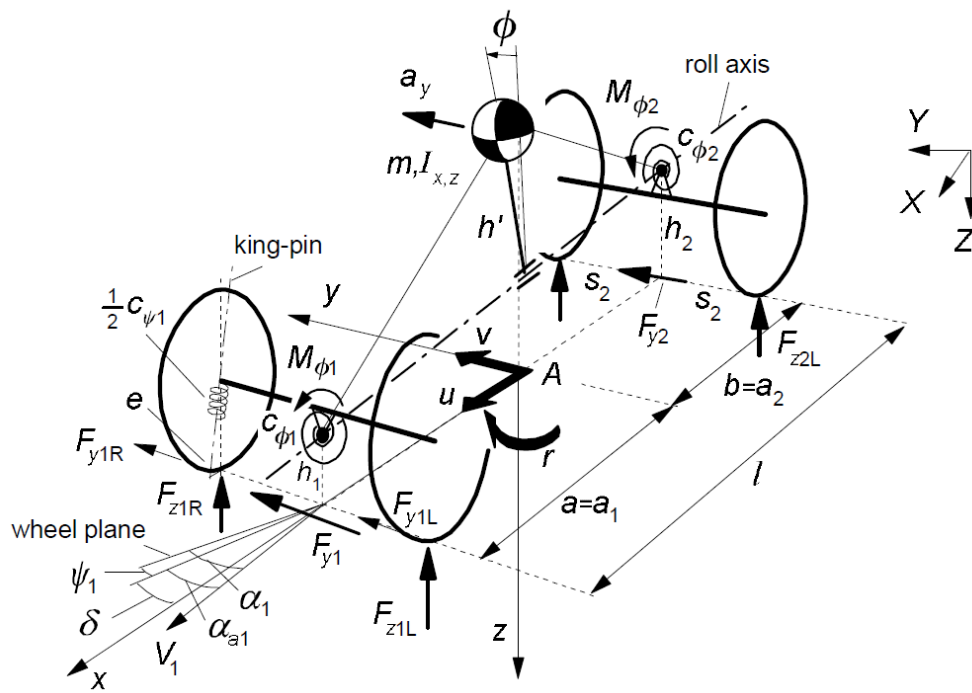


Figure 3.1: A two track model with 3 DOF; lateral, yaw & roll (Pacejka, 2012 [3])

3.1.1 Load transfer

The normal load on each tire is governed by a number of vehicle specific parameters, namely the mass and center of gravity position, and the front/rear roll couple distribution. The acceleration acting on the car then of course governs the load on each wheel. Equation 3.1 describes a simplification of the individual wheel normal load, with a steady state assumption and longitudinal acceleration neglected.

$$F_{ZFL} = m \left[\frac{g l_r}{2 L} - a_y \left(\frac{h_{RCf} l_r}{L w} + \frac{\Delta h}{w} \frac{c_{fw}}{c_{fw} + c_{rw}} \right) \right] \quad (3.1a)$$

$$F_{ZFR} = m \left[\frac{g l_r}{2 L} + a_y \left(\frac{h_{RCf} l_r}{L w} + \frac{\Delta h}{w} \frac{c_{fw}}{c_{fw} + c_{rw}} \right) \right] \quad (3.1b)$$

$$F_{ZRL} = m \left[\frac{g l_r}{2 L} - a_y \left(\frac{h_{RCr} l_f}{L w} + \frac{\Delta h}{w} \frac{c_{rw}}{c_{fw} + c_{rw}} \right) \right] \quad (3.1c)$$

$$F_{ZRR} = m \left[\frac{g l_r}{2 L} + a_y \left(\frac{h_{RCr} l_f}{L w} + \frac{\Delta h}{w} \frac{c_{rw}}{c_{fw} + c_{rw}} \right) \right] \quad (3.1d)$$

with

m	Vehicle mass
g	Acceleration due to gravity
l_f	Distance from CoG to front axle
l_r	Distance from CoG to rear axle
L	Wheelbase
w	Track width
Δh	Distance from roll center to CoG
a_y	Lateral acceleration
h_{RCf}	Front roll center height
h_{RCr}	Rear roll center height
c_{fw}	Front roll stiffness
c_{rw}	Rear roll stiffness

Lateral load transfer will also cause the vehicle to roll. The roll angle is dependent of the roll axis together with the total roll stiffness of the vehicle. Equation 3.2a shows the sprung mass roll angle. In addition the tires will also deflect giving an addition to the roll angle as in equation 3.2b. This equation assumes flat road and an infinitely stiff chassis. The tire deflection can be approximated either with the vertical tire stiffness or the relationship described in the Magic Formula (equation A.5). The total roll angle

relative to the road plane is simply the two contributions added together.

$$\phi_{SM} = \frac{m_s a_y}{k_\phi} \Delta h \quad (3.2a)$$

$$\Delta\phi_{tire} = \arcsin\left(\frac{\Delta z_r - \Delta z_l}{w}\right) \quad (3.2b)$$

$$\phi_{road} = \phi_{SM} + \Delta\phi_{tire} \quad (3.2c)$$

where

ϕ_{SM}	Body roll angle relative to wheel centers
$\Delta\phi_{tire}$	Roll angle due to tire deflection
ϕ_{road}	Total roll angle
m_s	Vehicle sprung mass
k_ϕ	Total roll stiffness
$\Delta z_{l/r}$	Left/Right wheel travel

3.1.2 Wheel orientation

Two other variables of high importance is the wheel steer and camber angle. The wheel angles are governed by the suspension kinematics of the specific axle, together with the compliance due to bushings and flexible suspension members. Assuming a linear camber behavior due to wheel travel, steer angle, and forces and moments acting on the wheel, gives equation 3.3. The camber angle to the road plane, which is here the angle of interest, also has to take the vehicle roll angle into consideration. An equation for the wheel steer angle is seen in 3.4. The steering ratio is here assumed to be constant, as well as the compliance behavior.

$$\gamma_{SM} = \gamma_0 + k_\delta \Delta\delta + k_z \Delta z + \mathbf{k}_{F\gamma} \bullet \Delta\mathbf{F} + \mathbf{k}_{M\gamma} \bullet \Delta\mathbf{M} \quad (3.3a)$$

$$\gamma_{road} = \gamma_{SM} \pm \phi_{road} \quad (3.3b)$$

$$\delta_{wheel} = \delta_0 + k_{SW} \delta_{SW} + \mathbf{k}_{F\delta} \bullet \Delta\mathbf{F} + \mathbf{k}_{M\delta} \bullet \Delta\mathbf{M} \quad (3.4)$$

with

3.1. VEHICLE MODELING

γ_{SM}	Camber angle to sprung mass
γ_{road}	Camber angle to road plane
δ_{wheel}	Wheel steer angle
γ_0	Static camber angle
δ_0	Static toe angle
k_δ	Camber change from wheel steer
k_z	Camber change from wheel travel
$\Delta\delta$	Change in wheel steer angle from static toe
Δz	Jounce travel from static ride height
$\mathbf{k}_F\gamma/\delta$	Camber/Steer angle stiffness due to forces on wheel
$\mathbf{k}_M\gamma/\delta$	Camber/Steer angle stiffness due to moments on wheel
\mathbf{F}	Force vector acting on wheel
\mathbf{M}	Moment vector acting on wheel
k_{SW}	Steer ratio
δ_{SW}	Steering wheel angle

In more advanced models the kinematics and compliance is no longer assumed have a linear influence of the wheel angles. Instead lookup tables can be used, that interpolate angles as a function of wheel position and load. The lookup tables can then be calibrated in K&C-machines, either virtually or on physical vehicles. Equation 3.5 shows such a relationship. This is the method being used in VI-CarRealTime.

$$\delta_{wheel} = \delta_0 + \Delta\delta_{SW}(SWA) + \Delta\delta_z(z) + \Delta\delta_F(\mathbf{F}) + \Delta\delta_M(\mathbf{M}) \quad (3.5a)$$

$$\gamma_{SM} = \gamma_0 + \Delta\gamma_z(z) + \Delta\gamma_\delta(\delta_{wheel}) + \Delta\gamma_F(\mathbf{F}) + \Delta\gamma_M(\mathbf{M}) \quad (3.5b)$$

where

$\Delta\delta_{SW}(SWA)$	Steer angle due to steering wheel angle
$\Delta\delta_z(z)$	Steer angle due to wheel jounce
$\Delta\delta_F(\mathbf{F})$	Steer angle due to forces acting on wheel
$\Delta\delta_M(\mathbf{M})$	Steer angle due to moments acting on wheel
$\Delta\gamma_z(z)$	Camber angle due to wheel jounce
$\Delta\gamma_\delta(\delta)$	Camber angle due to wheel steer
$\Delta\gamma_F(\mathbf{F})$	Camber angle due to forces acting on wheel
$\Delta\gamma_M(\mathbf{M})$	Camber angle due to moments acting on wheel

In a similar manner as for the wheel angles, the wheel position in X and Y also changes with wheel load, angles and jounce. In accordance with the reference systems used

in the magic formula, the wheel position is referenced by the intersection between the ground plane, the XZ wheel symmetry plane and the YZ wheel symmetry plane (ISO-W reference system, Chapter 2.2). The position of a wheel relative to a fix point on the vehicle is given in equation 3.6a, to the ISO-C reference system (origin in the hub). The translation to the wheel coordinate system is then shown in equation 3.6b. This equation assumes a linear behavior due to jounce, steer angle and loads effecting the wheel. A more accurate description can be seen in equation 3.7, where the behavior is instead captured in lookup-tables as in the wheel angle case. Once again, this is the method used in VI-CarRealTime.

$$\mathbf{r}_{C/0} = \mathbf{r}_{C0/0} + \mathbf{k}_z \Delta z + \mathbf{k}_\delta \Delta \delta + \mathbf{k}_F \Delta \mathbf{F} + \mathbf{k}_M \Delta \mathbf{M} \quad (3.6a)$$

$$\mathbf{r}_{W/0} = \mathbf{r}_{C/0} + R_e \begin{pmatrix} -\sin(\delta_{\text{wheel}}) \sin(\gamma_{\text{SM}}) \\ \cos(\delta_{\text{wheel}}) \sin(\gamma_{\text{SM}}) \\ -\cos(\gamma_{\text{SM}}) \end{pmatrix} \quad (3.6b)$$

$$\mathbf{r}_{C/0} = \mathbf{r}_{C0/0} + \Delta \mathbf{r}_z(z) + \Delta \mathbf{r}_\delta(\delta) + \Delta \mathbf{r}_F(F) + \Delta \mathbf{r}_M(M) \quad (3.7)$$

where

$\mathbf{r}_{C/0}$	Position vector from fixed point on vehicle to wheel center
$\mathbf{r}_{C0/0}$	Static position vector from fixed point on vehicle to wheel center
\mathbf{k}_z	Wheel position change due to jounce
\mathbf{k}_δ	Wheel position change due to wheel steer
\mathbf{k}_F	Wheel position change due to forces acting on wheel
\mathbf{k}_M	Wheel position change due to moments acting on wheel
R_e	Effective rolling radius

3.2 Magic Formula Tire Model

The Magic Formula is a semi-empirical tire model used to describe tire forces and moments generated as a function of slip angle, slip ratio, normal load and camber angle. The work in this research only applies to lateral pure slip conditions (the longitudinal slip ratio is zero). In its most simplistic form, the inputs and outputs to the Magic Formula for pure slip conditions is shown in Figure 3.2 below. (Pacejka, 2012 [3])

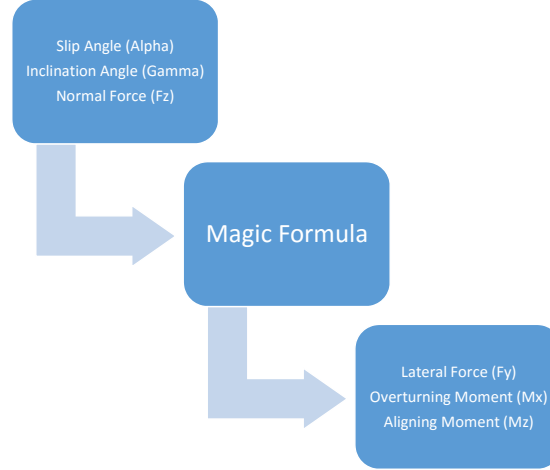


Figure 3.2: Inputs and outputs of the Magic Formula for pure slip

The formula in its most general form is described in equation 3.8. It holds true for a specific normal load and camber angle. y can represent F_x or F_y , and x can therefore represent either slip angle α , or slip ratio κ . Figure 3.3 shows a graphical explanation of the formula. The D parameter is the maximum value that the formula will take. $B \times C \times D$ equates to the slope at the origin, i.e. the cornering stiffness. C is the shape factor that governs the shape of the curve. B is called the stiffness factor and is left to control the cornering stiffness. E is the curvature factor which governs the shape and horizontal position of the peak. To account for non-symmetric tire behavior, S_V and S_H (the vertical and horizontal shifts) are included. They are simply constants that move the curve in the X and Y -direction.

$$y = D \sin [C \arctan \{B x - E (B x - \arctan(B x))\}] \quad (3.8a)$$

$$Y(X) = y(x) + S_V \quad (3.8b)$$

$$x = X + S_H \quad (3.8c)$$

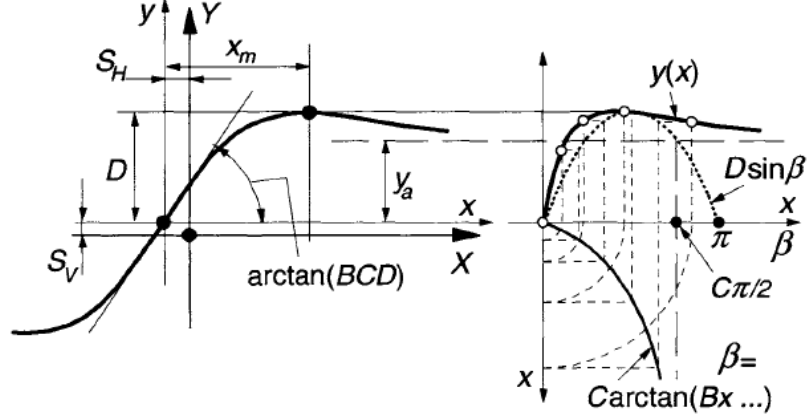


Figure 3.3: Illustration of Magic Formula parameters (Pacejka, 2012 [3])

To account for tire influences from normal load and camber angle, the equations need to be expanded significantly. New equations for the parameters B , C , D and E are included, where factors for camber angle influence and normal load sensitivity are incorporated. Two of the most important parts of the lateral force equations in the Magic Formula, the cornering stiffness and maximum friction equations, can be seen in equation 3.9. In total there are 12 steady state lateral force equations, and 19 aligning moment equations. In the 12 lateral force equations there are 18 different parameters that make up a particular tire. Similarly, for the aligning moment equations there are another 25 parameters. The complete steady state equations for lateral forces and moments can be found in Appendix A.2.

Maximum friction and cornering stiffness equations (Pure side slip):

$$\mu_y = \frac{(p_{Dy1} + p_{Dy2} df_z) (1 - p_{Dy3} \gamma^{*2}) \lambda_{\mu y}}{1 + \lambda_{\mu V} V_s/V_0} \quad (3.9a)$$

$$K_{y\alpha 0} = p_{Ky1} F'_{z0} \sin [2 \arctan \{F_z / (p_{Ky2} F'_{z0})\}] \lambda_{Ky\alpha} \quad (3.9b)$$

$$K_{y\alpha} = K_{y\alpha 0} (1 - p_{Ky3} \gamma^{*2}) \xi_3 \quad (3.9c)$$

3.2.1 Slip angles

The slip angles of all individual wheels are crucial for an accurate representation of the tire. It is defined as the angle between the wheel heading and its velocity vector. The velocity of a point p relative to a point 0 is defined in equations 3.10. Since all measurements are done in a steady state assumption, equation 3.10b is assumed to be

3.2. MAGIC FORMULA TIRE MODEL

small enough to be neglected.

$$\mathbf{v}_p = \mathbf{v}_o + \mathbf{v}_{rel} + \boldsymbol{\omega} \times \mathbf{r}_{p/o} \quad (3.10a)$$

$$\mathbf{v}_{rel} = \frac{d}{dt} \mathbf{r}^{W/o} \quad (3.10b)$$

where

- \mathbf{v}_p Velocity vector at point p
- \mathbf{v}_o Velocity vector at point 0
- $\boldsymbol{\omega}$ Rotational velocity vector
- $\mathbf{r}_{p/o}$ Position vector from 0 to p

When the wheel velocity is known, the slip angle can then be calculated as in equation 3.11. All velocities are still in the vehicle axis system.

$$\alpha = \delta_{wheel} - \arctan\left(\frac{v_y}{|v_x|}\right) \quad (3.11a)$$

$$\mathbf{v}_p = \begin{pmatrix} v_x \\ v_y \\ v_z \end{pmatrix} \quad (3.11b)$$

4

Using the Vehicle as a Tire Testing Machine

4.1 Limitations of In-vehicle Measurements

When conducting tire testing on a Flat-Trac machine, one has the advantage of being able to independently manipulate the variables that influence a tire's behavior. A sample Flat-Trac dataset is shown in Figure 4.1. As can be seen, a wide range of data is possible to collect with this method, allowing a tire model to be created that is accurate over a wide range of slip angles, normal loads, and camber angles. Using measurements from in-vehicle testing does not allow for such a luxury. In this thesis, the forces and moments in all three local reference axes $(XYZ)_C$ are measured. The target is to achieve sufficient tire load cases and measure all necessary data to be able to accurately fit the Magic Tire formula. There are several difficulties to overcome in this process.

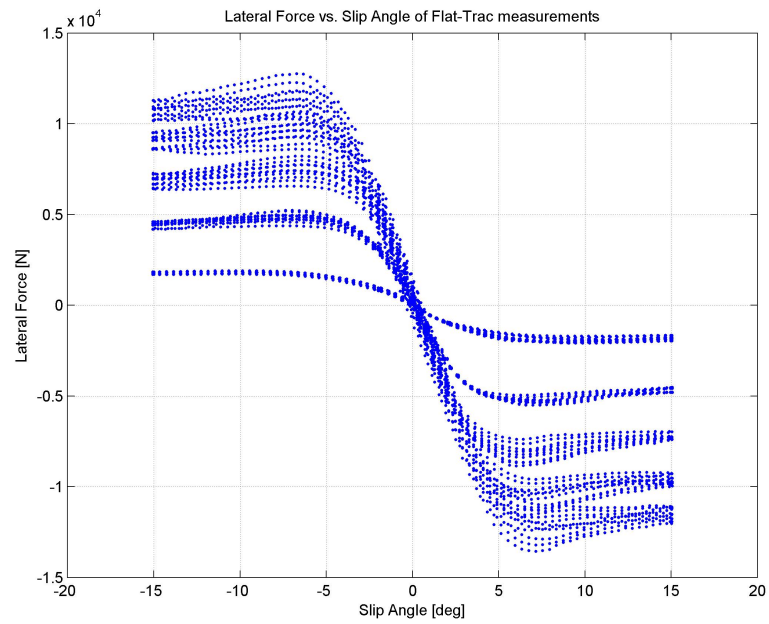


Figure 4.1: Lateral force vs. slip angle of Flat-Trac measurement data for several different normal loads and camber angles

As a comparison, a dataset collected from in-vehicle measurements is shown in Figure 4.2 that highlights the regions of data that are difficult to collect without a Flat-Trac rig.

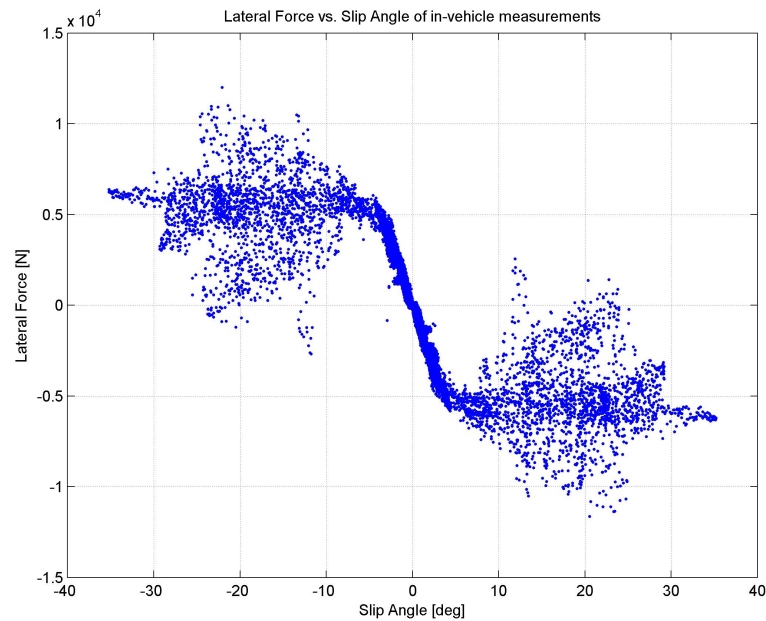


Figure 4.2: Lateral force vs. slip angle of in-vehicle measurement data for several different normal loads and camber angles. Data has been mirrored to represent a typical dataset.

4.1.1 Load transfer

By using a vehicle as the test machine, the normal loads that can be measured are limited to what can be achieved by the static normal loading of the tires, plus the load transfer that occurs during lateral acceleration. Unfortunately, since the load transfer is proportional to lateral acceleration, the individual wheel loads in steady state cornering are mostly defined by the vehicle mass, center of gravity location, and roll stiffness distribution. This means that for any given lateral acceleration, each wheel will have a certain normal load. This is an issue because it means that during high lateral acceleration the inner wheels will have high slip angles and low normal loads, the outer wheels will have high slip angles and high normal loads, but it becomes hard to capture high slip angles together with normal loads near the static normal loading of the tires. This can easily be seen in Figure 4.3 showing simulation results of a quasi steady-state vehicle maneuver, where data is lacking for normal loads between 2000N and 6000N for slip angles in the non-linear region of the tire. Because of this, it is beneficial to have a vehicle with a large difference in mass distribution between the front and rear axles, in order to capture the greatest range of data.

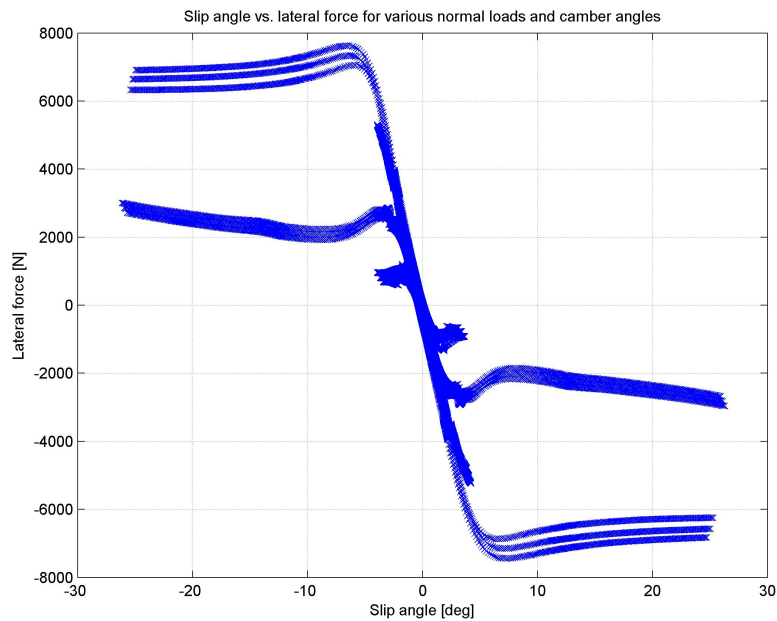


Figure 4.3: Lateral force vs. slip angle of VI-CarRealTime simulations

4.1.2 Wheel orientation

As a vehicle enters steady state cornering, the vehicle will roll. If the camber gain of the wheel due to kinematics and compliance is less than the amount of body roll (which is almost always the case on production vehicles), the wheel's orientation will go towards positive camber. This makes it very hard to capture data with high load, high slip angle, and negative camber angle. In order to achieve this, three different static camber angle settings were tested on the vehicle. This includes an exaggerated negative static camber angle, factory static camber setting, and even a positive static camber angle set on the vehicle.

4.1.3 Slip angles

To keep the test method safe, predictable, and repeatable, it was chosen to only achieve high slip angles on the front axle. By having an understeered vehicle, most of the data that is gathered in the non-linear range is from the front axle, so the normal loads that are able to be measured during high slip angles are those of the front axle with load transfer.

4.2 Simulations

Simulations were run using a Volvo V40 Cross Country model in VI-CarRealTime, to create a realistic dataset for verification on whether fitting a Magic Formula tire model would be possible at all from in-vehicle measurements. VI-CarRealTime uses a two-track model with symbolically derived equations of motion, described in Chapter 3.1. Suspension and steering kinematics and compliance is superimposed from look-up tables, which have been configured to match the results from a K&C test of the V40. The tires are modeled using Pacejka's Magic Formula, using the PAC2002 standard (Chapter 3.2).

A demand on the testing procedures was that it should capture slip angles well beyond the linear range of the tire, in order to capture its asymptotic behavior. There was also a need to capture a wide range of camber angles to accurately apprehend the effects on the tire due to the camber angle. To reduce the influence of transient effects in the measurements, higher longitudinal speeds were also preferable for the tests. Ideally the tests should also closely resemble realistic driving maneuvers, to not have high heat build up in the tire, which would affect maximum friction as well as cornering stiffness. Lastly, a set of constraints also existed from the physical dimensions of the handling areas at Hällered Proving Ground (Figure 1.3).

It was decided that the tests should be divided into two major sections: one for the linear range only, and the other for the non-linear range. In order to capture a wide enough range of camber angles, the tests were to be conducted with different static camber angles. The magnitude of these was constrained by the available space in the car, and what modifications were realistic to conduct. It was decided to go for three different increments of static camber: -3, 0, and 3 degrees. Since many tires are not symmetric, it was also decided to capture the shifts associated with this behavior by mirroring the tires.

4.3 Design of Vehicle Maneuvers & Procedures

Due to constraints on the size of the available areas for testing, it was decided to run all tests at the skidpad at Hällered Proving Ground (Figure 1.3). A drawback with skidpad testing is that it does not resemble a realistic driving scenario, leading to excessive tire heat build up. It is therefore of importance to keep the maneuvers short, and to carefully monitor the tire temperatures between the tests so that no residual heat affects the results. Furthermore, it is also preferable to run the tests at the highest possible forward velocity, in order to minimize the transient effects. The tests are therefore executed on the outermost radius of the skidpad.

4.3.1 Required Data range

In order to have Magic Tire model parameters that accurately represent a tire, there is a requirement to have a wide range of slip angles, normal loads, and camber angles. Normal Flat-Trac datasets sweep slip angles from -15 to $+15$ degrees using 3 or more constant normal loads, each with 3 or more constant inclination angles of the wheel. From fitting simulated datasets, it was found that having a greater range of slip angles helped the accuracy of the fitted model, as well as prevented unwanted constraint violations in the model.

4.3.2 Linear Maneuver

The linear test is run on the outermost radius on the skidpad, 50m. To maintain load cases as close as possible to steady state, the car should be accelerated at 0.4m/s^2 longitudinally, while maintaining a constant turning radius. The test is executed until the front tires start to saturate, at a slip angle of approximately $3 - 4^\circ$. The achieved slip angles, camber angles, and normal loads can be seen in Figures 4.4-4.6. Note that the wheel angles are given in the wheel coordinate systems, therefore the left and right wheels will have opposite signs for both slip angle and steered angle. The normal load is dictated by the physical properties of the vehicle, such as center of gravity position and roll stiffness distribution, and the camber angles are dependent on the kinetic behavior of the suspension system and the static camber angles. If testing is to be conducted on a vehicle, there is no easy way of extending the range of these parameters.

4.3. DESIGN OF VEHICLE MANEUVERS & PROCEDURES

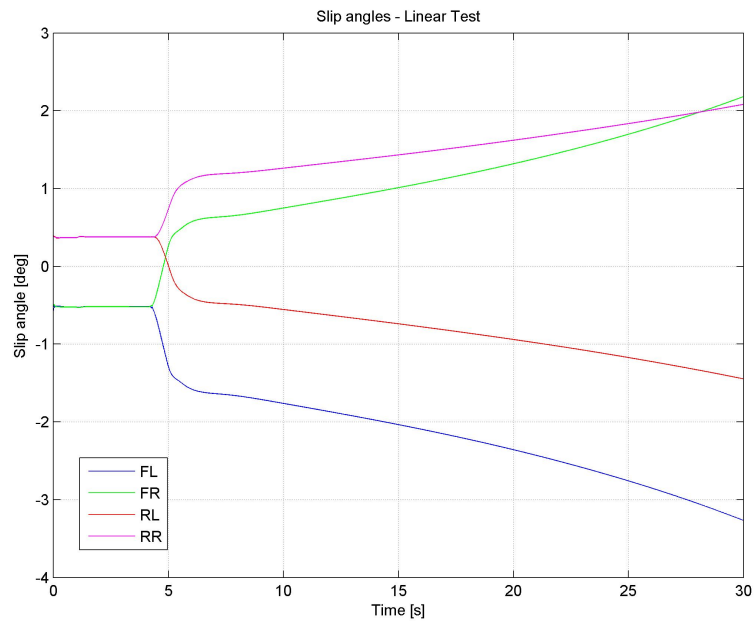


Figure 4.4: Simulated slip angles during linear maneuver

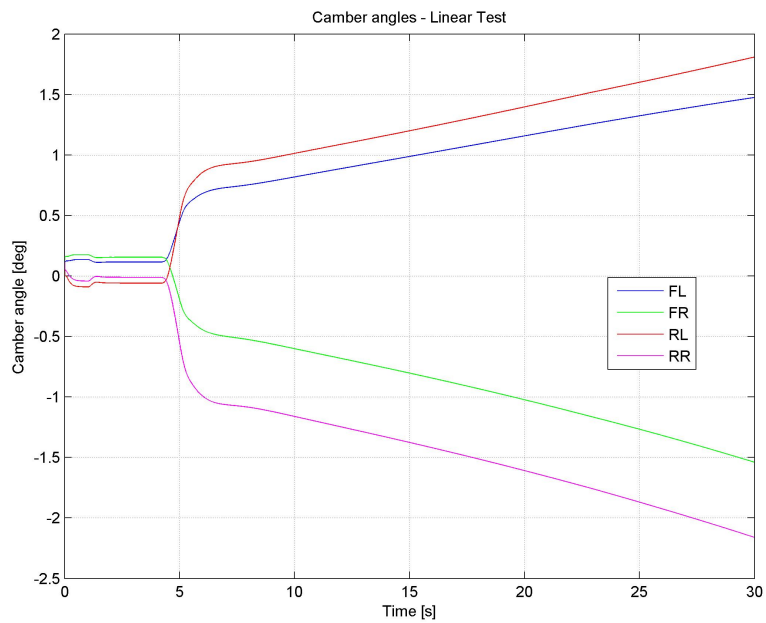


Figure 4.5: Simulated camber angles during linear maneuver

4.3. DESIGN OF VEHICLE MANEUVERS & PROCEDURES

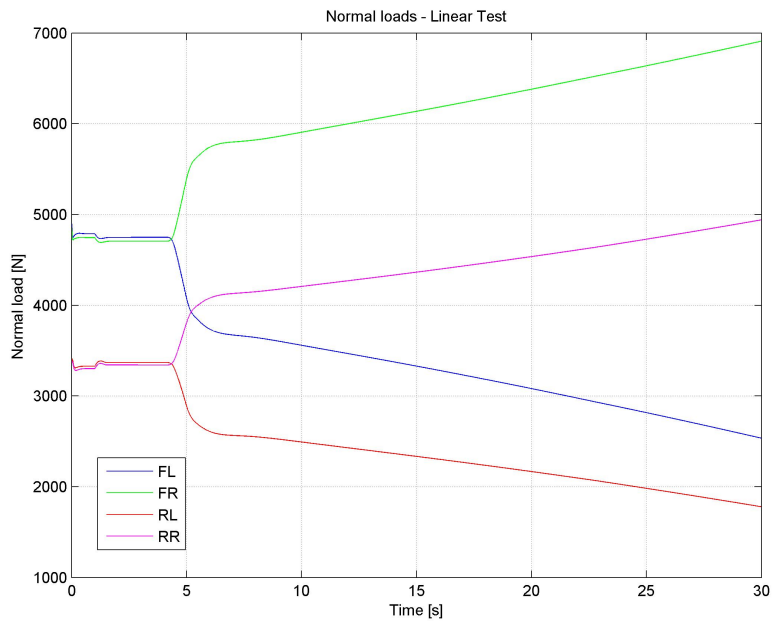


Figure 4.6: Simulated normal loads during linear maneuver

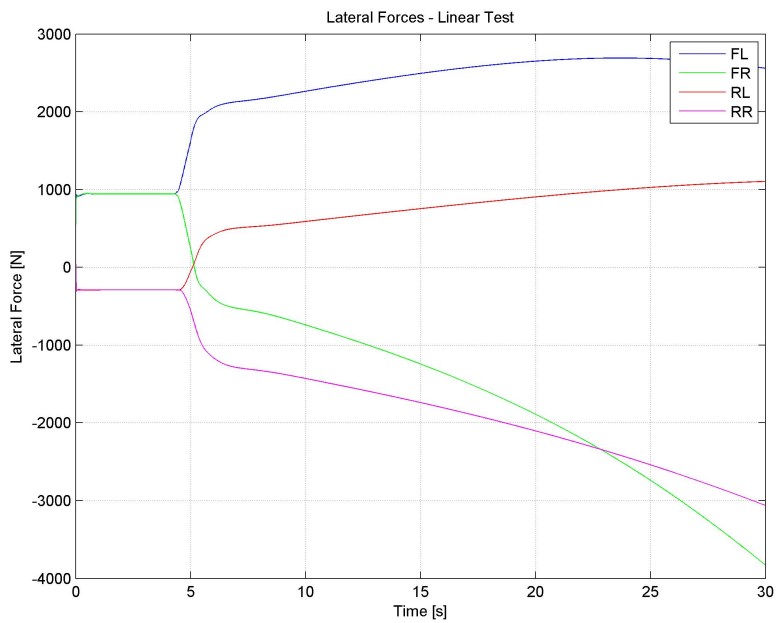


Figure 4.7: Simulated lateral forces during linear maneuver

4.3.3 Non-Linear maneuver

The non-linear maneuver starts at the outermost radius on the skidpad. The purpose of this test is to capture the tire properties after the tire saturates. To minimize heat build-up in the tires, the vehicle is quickly taken up to the lateral limit of the tires. The clutch is then engaged to minimize the combined slip, and the steering wheel angle is increased in a linear fashion to reach steering lock in 4 seconds. This makes the vehicle understeer, with slip angles up to 25° . An understeered vehicle is of course a necessity for this test. If the vehicle would be oversteered this maneuver would trigger an unstable behavior, making it hard to control the vehicle through the maneuver, which would therefore lead to bad control of the variables. The test gives a large amount of data to determine the asymptotic behavior of the tire (Figure 4.8). The normal load on the tires is relatively constant owing to that the lateral force for most street tires is fairly constant with slip angles in the saturated region (Figure 4.11).

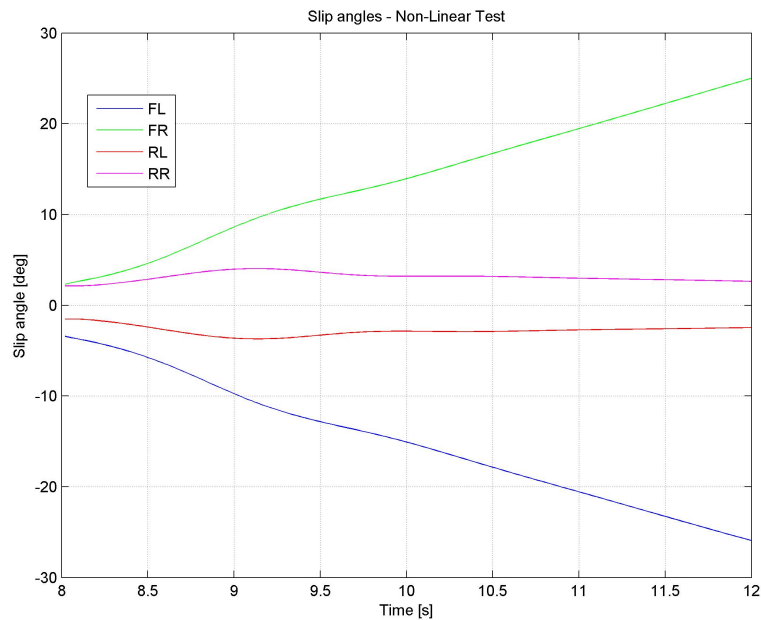


Figure 4.8: Simulated slip angles during non-linear maneuver

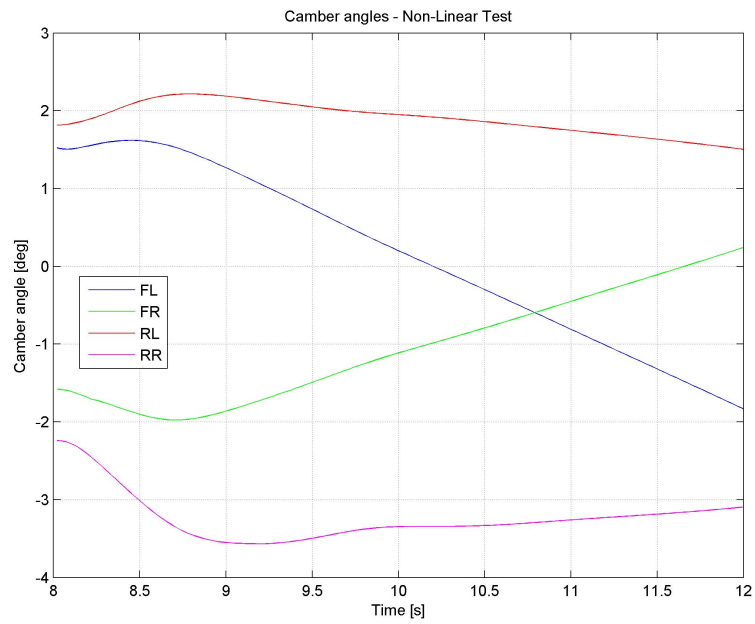


Figure 4.9: Simulated camber angles during non-linear maneuver

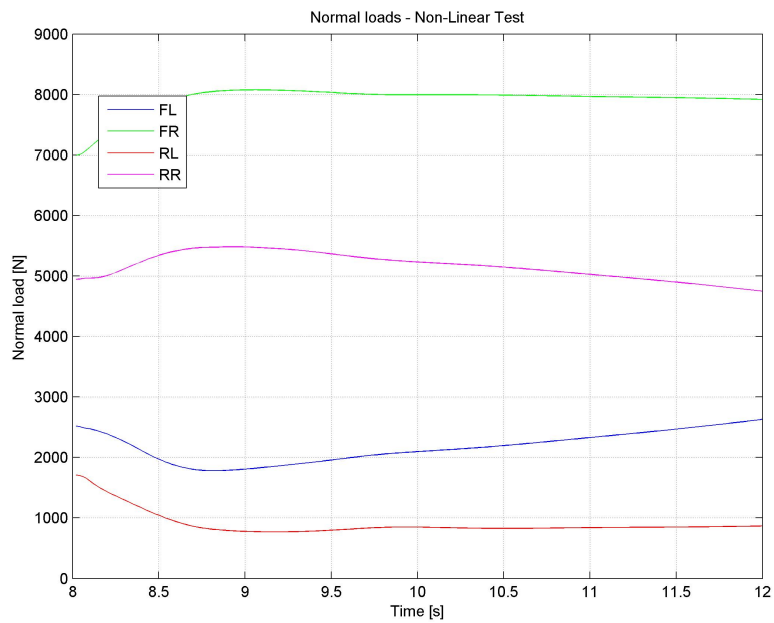


Figure 4.10: Simulated normal loads during non-linear maneuver

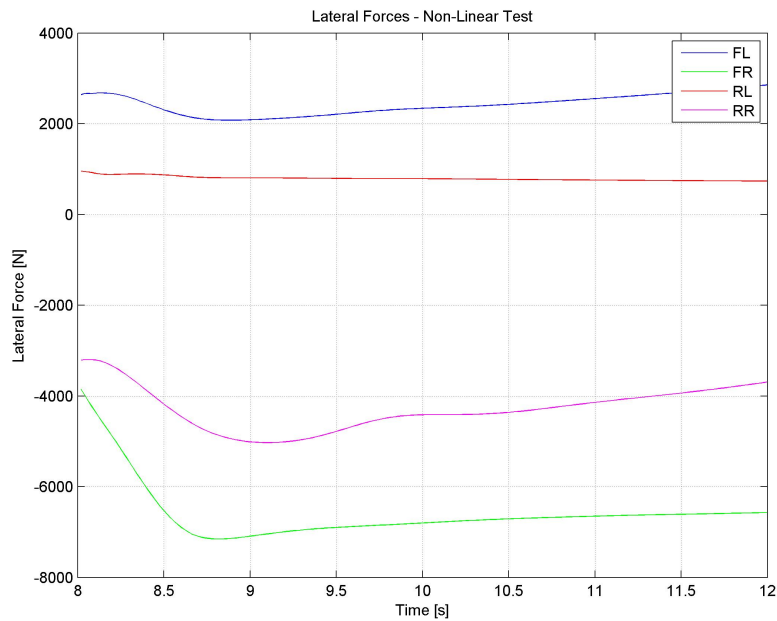


Figure 4.11: Simulated lateral forces during non-linear maneuver

4.4 Vehicle Preparation

The vehicle that was chosen for physical testing was a 2013 Volvo V40 CC. This vehicle was chosen because of the good correlation between the existing full vehicle model in VI-CarRealTime and results from real driving maneuvers. Several modifications were done to the car in order to allow the adjustment of static camber through the required range determined by the simulation results for the test procedures.

4.4.1 Front Camber Adjustment

The Volvo V40 uses a McPherson strut front suspension, shown in Figure 4.12.

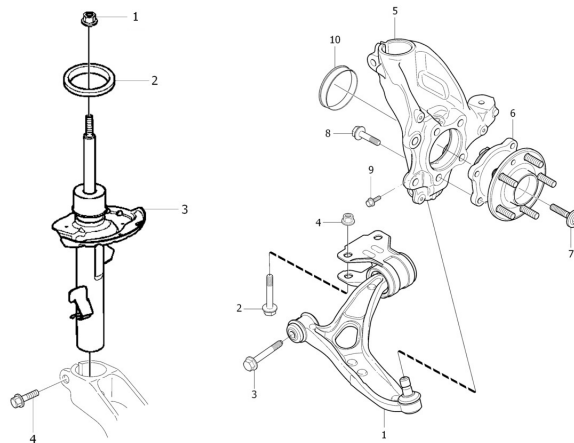


Figure 4.12: Volvo V40 front suspension

The static camber is adjusted by moving the strut top mount laterally. In the original configuration, no camber adjustment was available, so camber adjustment plates were designed to allow the strut top to be moved inwards as well as outwards from the original mounting position. Since the camber adjustment plates have three discrete options for static camber settings, repeatability between configuration changes is good. These camber adjustment plates were designed using CATIA, and can be seen in Figure 4.13.

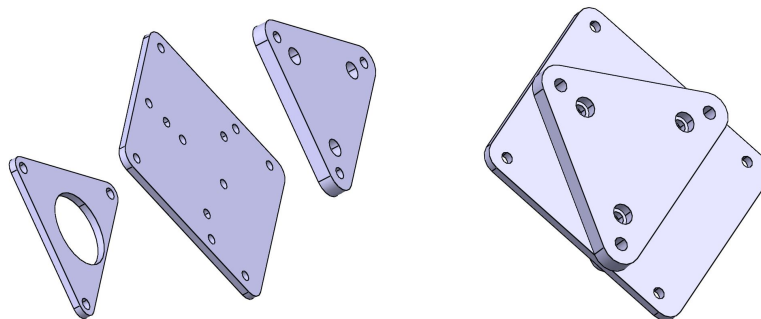


Figure 4.13: CAD model of camber adjustment plates

Since the outer diameter of the original front coil spring was 160mm, clearance between the spring and vehicle body would not have been maintained when static camber was adjusted to the maximum negative camber setting. Because of this, the original struts were modified to accept a standard 2.5" inner diameter racing spring. The new spring was chosen to match the behavior of the original spring as closely as possible, and can be seen in Table 4.1.

4.4. VEHICLE PREPARATION

Spring	Rate [N/mm]	Free length [mm]	OD [mm]
Original	28.5	315	160
Racing	28.9	305	90

Table 4.1: Specifications for original and racing springs

The original lower spring seat was replaced with a machined aluminum spring seat to match the smaller diameter springs. Since the strut top bearing was only suitable for the larger diameter original coil spring, a new upper spring seat assembly was designed which uses a Volvo 740 strut bearing, seen in Figure 4.14.



Figure 4.14: Machined strut bearing assembly

The Chalmers Prototype Lab provided the tools and machinery necessary to manufacture the new parts and install them on the original struts, which can be seen in Figures 4.15 and 4.16.



Figure 4.15: Modified Volvo V40 struts and camber adjustment plates



Figure 4.16: Modified Volvo V40 struts installed on vehicle

After installing the modified struts and camber adjustment plates on the vehicle, the required static camber adjustment range was achieved. The static camber settings for the front axle are given in Table 4.2 as measured on the wheel alignment rack at Hällered Proving Ground.

Setting	Camber Angle [°]	
	Left	Right
Negative	-3.04	-3.17
Neutral	-0.75	-0.76
Positive	+3.06	+2.88

Table 4.2: Front static camber angles

4.4.2 Rear Camber Adjustment

The rear suspension on the Volvo V40 is of the independent trailing arm type. In original form there is inadequate adjustment for static camber, so modifications to the subframe were made to allow adjustment. It was chosen to change the upper link's hole in the subframe to a slot so that the link can be moved laterally. The hole to be modified is shown in Figure 4.17.

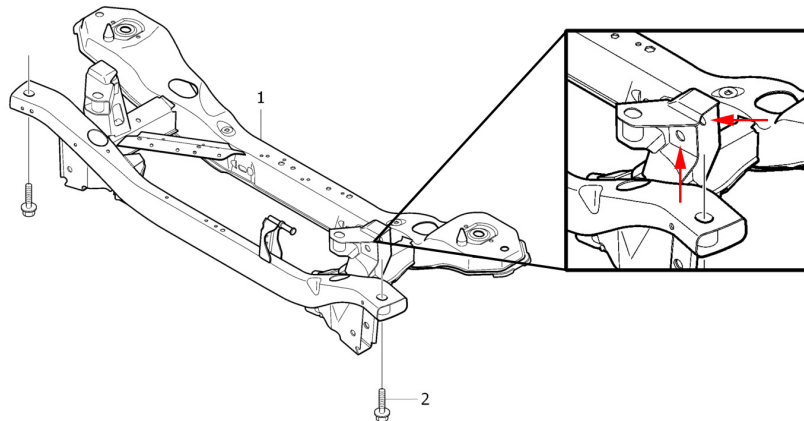


Figure 4.17: Volvo V40 rear subframe modifications

The rear subframe assembly was removed from the vehicle at Volvo and slots were made in place of the original holes. The static camber settings that were achieved on the rear axle are given in Table 4.3.

Setting	Camber Angle [°]	
	Left	Right
Negative	-3.12	-3.31
Neutral	-1.43	-1.44
Positive	+0.45	+0.45

Table 4.3: Rear static camber angles

4.5 Instrumentation

Several measurement sensors are used in order to record the necessary data to be used as inputs to the Magic Formula. While the wheel forces and moments are measured directly in the C-Axis system (Figure 2.1), the wheel angles need to be measured as well in order to transfer these into the W-Axis system (Figure 2.2). Furthermore, to calculate the slip angles of the tires the measured wheel angles need to be used together with the lateral and longitudinal velocities of the vehicle provided by the Inertial Measurement Unit (IMU). The sensors that are used to calculate the inputs to the Magic Formula are shown in Table 4.4.

Data Channel	Sensors
Lateral Force (F_y)	Wheel Force Transducers & Camera System
Normal Force (F_z)	Wheel Force Transducers & Camera System
Overturning Moment (M_x)	Wheel Force Transducers
Aligning Moment (M_z)	Wheel Force Transducers
Slip Angle (α)	Camera System & IMU
Camber Angle (γ)	Camera System

Table 4.4: Sensors used for measurement data channels

4.5.1 Data Acquisition System

A DEWESoft Sirius data logging system was installed in the vehicle. This set of hardware is responsible for monitoring and recording the data provided by the system of sensors installed throughout the vehicle.

4.5.2 Wheel Force Transducers

The measurement wheels used on the vehicle for testing were Kistler RoaDyn S660 units. These wheels house six equally spaced strain gauge load cells in order to measure the forces exerted on the hub at any given time. Wheel force transducers are required to measure the forces and moments at the wheel to create a tire model that truly represents the tire, rather than a tire model that only represents the effective axle characteristics. One of the four wheel force transducers is shown in Figure 4.18.



Figure 4.18: Kistler RoadDyn S660 wheel force transducer

The rotational orientation of the wheel is also monitored to measure camber and steered angles. This allows the forces and moments exerted on the wheel to be transformed into the ISO-C coordinate system. The wheels then transmit the data wirelessly to receivers mounted on each of the uprights, which in turn connect to the data logging system. The upright-mounted wireless receiver can be seen in Figure 4.19.

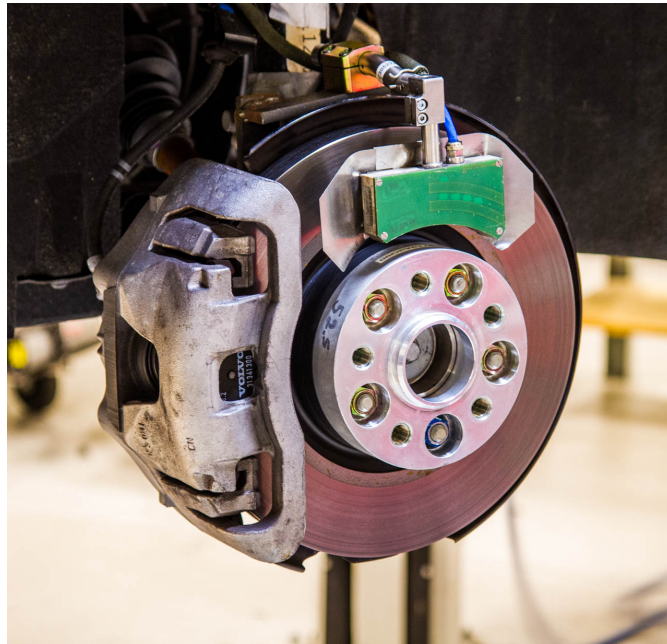


Figure 4.19: Wireless receiver for wheel force transducer

4.5.3 Inertial Measurement Unit

Since the vehicle velocity and yaw rate are required to calculate the slip angles at each of the four wheels, a combined IMU and GPS device were used to accurately resolve the states of the vehicle. An Oxford Technical Solutions RT-3002 IMU was installed in the vehicle to provide the velocity and yaw rate data channels. This precision device blends inertial measurements with GPS data in order to give the most accurate vehicle velocity and heading, especially in locations where the GPS signal is weak. Along with a standard GPS signal, the IMU uses a secondary signal from a base station at Hällered Proving Ground in order to maintain accuracy of 0.02m. The system updates at 100Hz to provide high bandwidth data to the logging system. The IMU is mounted in the passenger compartment of the vehicle behind the front seats, as shown in Figure 4.20.



Figure 4.20: Inertial measurement unit mounted in vehicle

4.5.4 Optical Wheel Measurement System

An Aicon WheelWatch camera system was installed on the vehicle in order to directly measure the wheel positions and angles. By measuring these variables directly, the error is reduced compared to using simulated wheel angles and positions as inputs to the Magic Formula tire model. The actual wheel displacements and angles can then also be compared to the simulated values in order to further verify the vehicle model if required. The WheelWatch system uses four high speed cameras mounted outboard of the vehicle that point towards the wheels being monitored. Reflective markers are fixed on the vehicle fenders as well as on discs attached to the wheels to provide the reference system. This camera system can accurately resolve changes in wheel position to 0.1mm, and has an angular accuracy of 0.015 degrees. The maximum update frequency of the system is 490Hz, which exceeds the requirements of this test method. An advantage to this non-contact method of measurement is that vibrations and movements of the measurement equipment do not affect the measurements. The camera system wheel angles were calibrated while the vehicle was on the laser alignment rack at Hällered Proving Ground before each test session. The WheelWatch camera and reference markers of the front right wheel are shown in Figure 4.21.



Figure 4.21: AICON WheelWatch camera system

4.5.5 Wheel Travel Transducers

To measure the vertical wheel travel in order to calculate the roll angle with respect to the road, position transducers were mounted on the suspension components at the four corners of the vehicle. This system provides a redundant system to the optical wheel measurement system for measuring wheel displacements, and allows the measured data from each system to be validated with each other.

4.5.6 CAN Bus

The data acquisition system was interfaced with the vehicle CAN bus in order to log the steering wheel angle and to allow for other channels to be logged if required.

4.6 In-Vehicle Measurements

4.6.1 Test Schedule

To reduce tire wear and keep tire temperatures as even as possible, the linear maneuvers were driven first for each camber setting, and then the non-linear maneuvers. It was planned to drive the car with the -3° static camber setting first, then the 0° setting, and finally the $+3^\circ$ setting in order to keep tire wear as even as possible. However, due to time constraints while testing, it was chosen to skip the 0° camber setting on the front

axle and skip the $+3^\circ$ setting on the rear axle. This allowed for measurements to be made in the non-linear range at the $+3^\circ$ setting, which is where positive camber is likely to occur. The complete test schedule can be seen in Table 4.5.

Test	Camber	Maneuver	Direction	Track Temperature
1	-3° F, -3° R	Linear	Left	40.1°C
2	-3° F, -3° R	Linear	Right	40.1°C
3	-3° F, -3° R	Linear	Left	40.1°C
4	-3° F, -3° R	Linear	Right	40.1°C
5	-3° F, -3° R	Non-Linear	Left	40.1°C
6	-3° F, -3° R	Non-Linear	Right	40.1°C
7	-3° F, -3° R	Non-Linear	Left	40.1°C
8	-3° F, -3° R	Non-Linear	Right	40.1°C
9	$+3^\circ$ F, 0° R	Linear	Left	36.7°C
10	$+3^\circ$ F, 0° R	Linear	Right	36.7°C
11	$+3^\circ$ F, 0° R	Non-Linear	Left	36.7°C
12	$+3^\circ$ F, 0° R	Non-Linear	Right	36.7°C
13	$+3^\circ$ F, 0° R	Non-Linear	Left	36.7°C
14	$+3^\circ$ F, 0° R	Non-Linear	Right	36.7°C

Table 4.5: Test schedule for driving maneuvers

4.6.2 Tire Temperatures

Tire temperature measurements were taken immediately after the test maneuvers were completed. The measurements were taken with a Fluke 66 infrared thermometer. The tire temperatures are given in Table 4.6.

Test	Tread Surface Temperature [°C]			
	FL	FR	RL	RR
Pre-Test	30.2	32.3	31.6	30.3
1	39.9	40.3	38.4	37.4
2	43.5	33.4	39.7	31.5
3	35.7	46.8	33.8	41.9
4	44.8	38.2	41.8	32.8
5	36.9	58.5	33.5	39.4
6	62.8	43.8	41.5	33.4
7	41.8	61.8	33.8	40.8
8	75.1	47.2	41.8	35.0
Pre-Test	24.9	26.2	24.2	23.1
9	34.7	43.2	29.5	35.7
10	41.3	37.9	34.5	31.4
11	41.3	60.1	31.8	38.2
12	59.2	45.6	40.3	32.9
13	45.3	66.5	32.2	38.4
14	72.7	51.6	39.7	33.4

Table 4.6: Tire temperatures taken after each test maneuver

4.6.3 Linear Maneuver

By conducting the vehicle maneuvers designed for this method of tire measurement, the required slip angle range was achieved, as can be seen in Figure 4.23. A photograph of the vehicle performing the linear maneuver is shown in Figure 4.22. The range of normal loads as dictated by the lateral load transfer can be seen in Figure 4.24. The wheel angles are shown in Figure 4.26. Slip angles and steered angles are in the wheel coordinate systems. The measurement results are as expected and match very closely with the simulated results (Section 4.3.2).



Figure 4.22: Vehicle performing linear range maneuver while instrumented with measurement equipment.

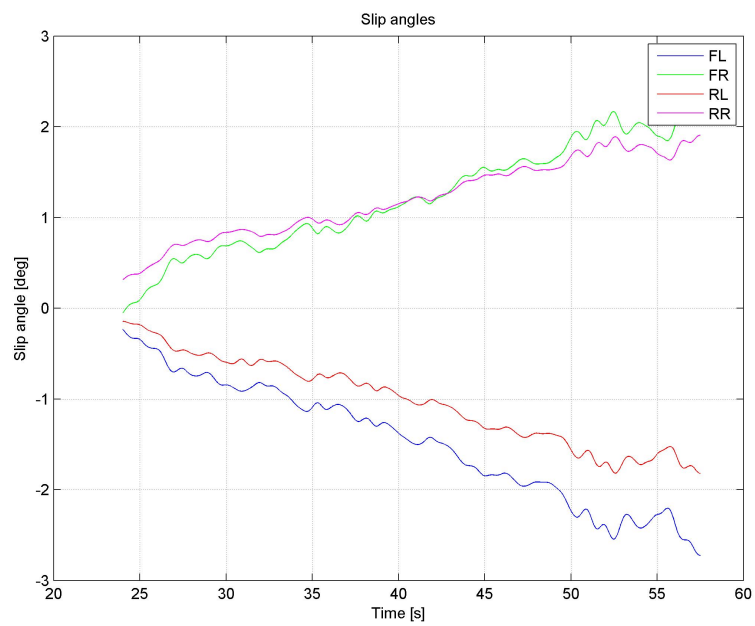


Figure 4.23: Slip angles during linear vehicle maneuver

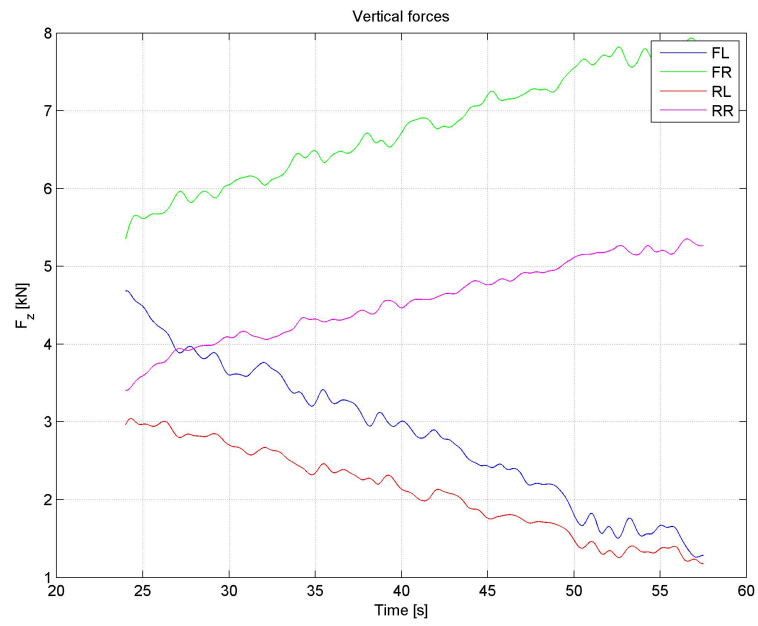


Figure 4.24: Normal loads during linear vehicle maneuver

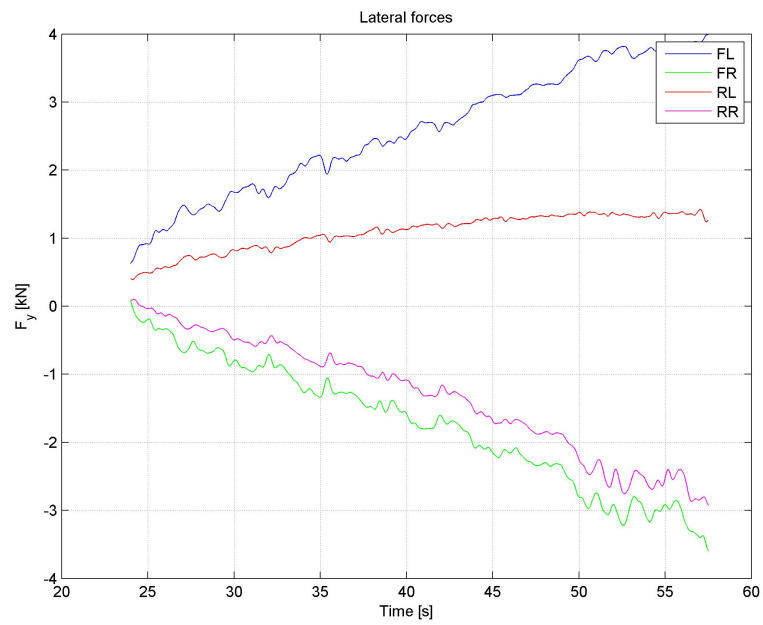


Figure 4.25: Lateral forces during linear vehicle maneuver

4.6. IN-VEHICLE MEASUREMENTS

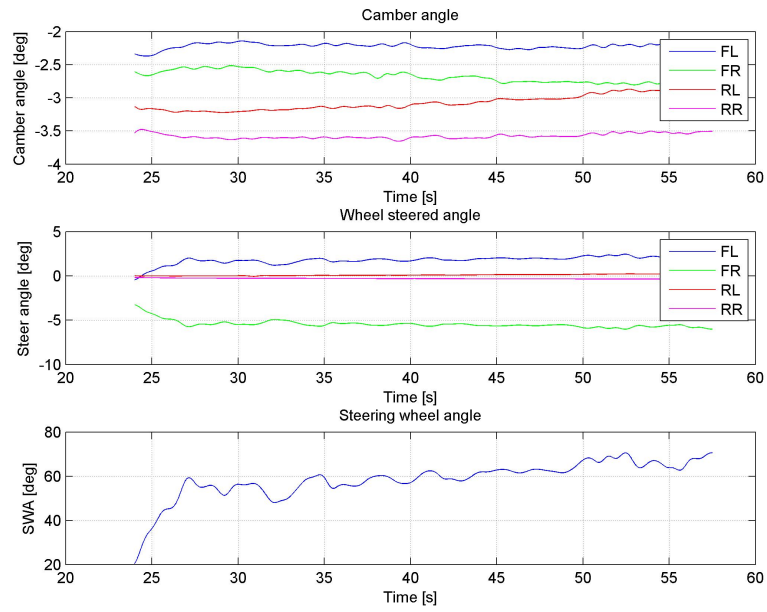


Figure 4.26: Wheel angles during linear vehicle maneuver

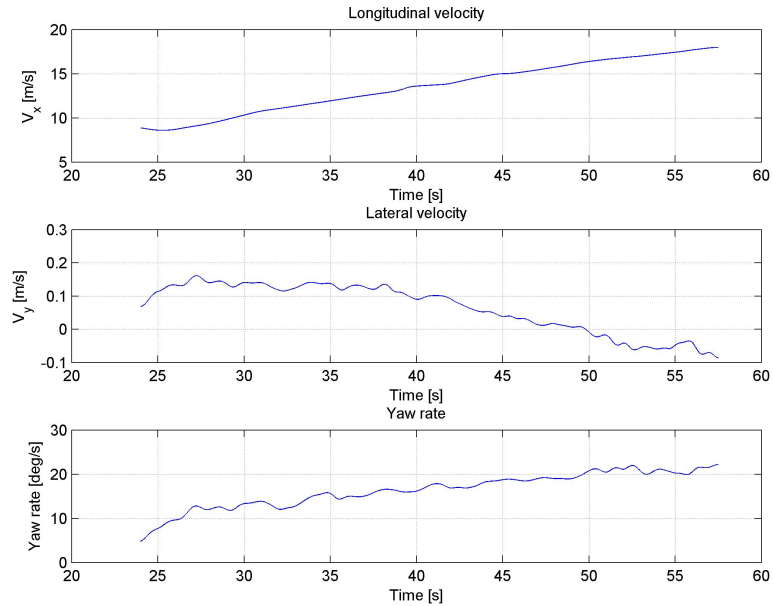


Figure 4.27: Vehicle velocities during linear vehicle maneuver

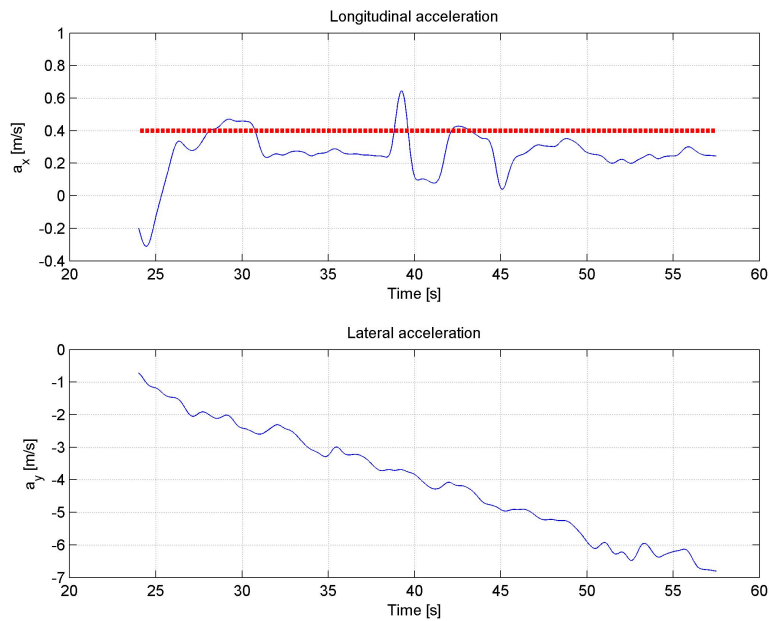


Figure 4.28: Vehicle accelerations during linear vehicle maneuver

4.6.4 Non-Linear Maneuver

The measurements for the non-linear maneuver can be seen in Figures 4.29 through 4.34. Slip angles and steered angles are in the wheel coordinate systems. The measurement results for the slip angles and normal loads match very closely with the simulated slip angles for the non-linear maneuver (Section 4.3.3). The measured lateral forces during the maneuver were less than what was expected based on the simulation results. In the simulations the right front tire produced in excess of 7000N, but in the measurements this tire only produced roughly 6000N. However, the behavior of the measurements during this maneuver in general is as expected.

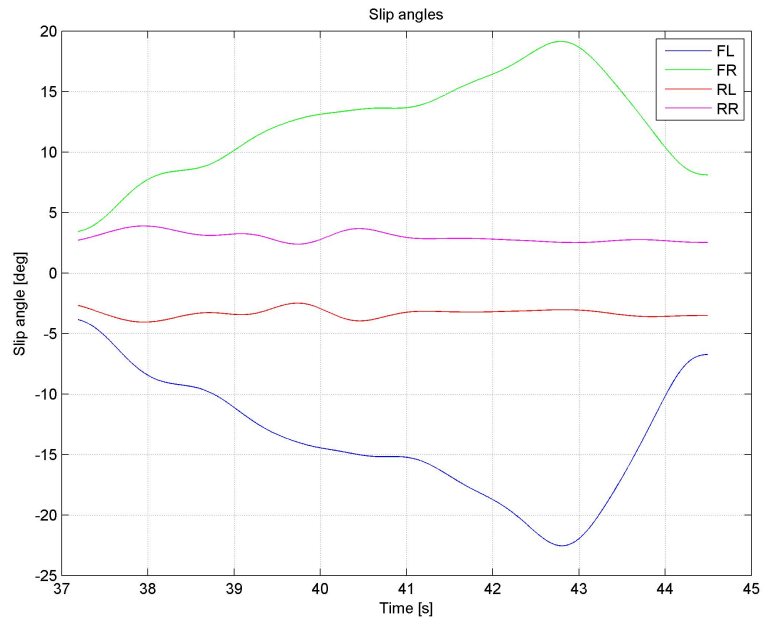


Figure 4.29: Slip angles during non-linear vehicle maneuver

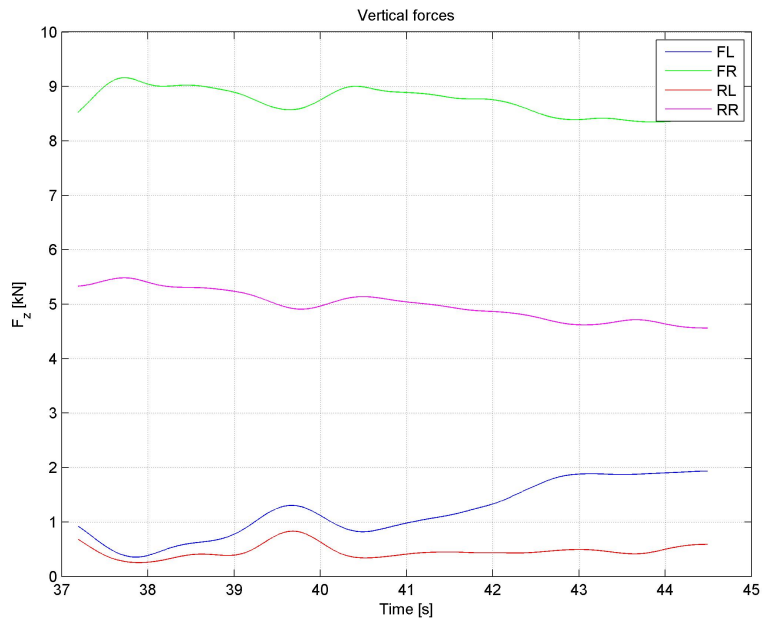


Figure 4.30: Normal loads during non-linear vehicle maneuver

4.6. IN-VEHICLE MEASUREMENTS

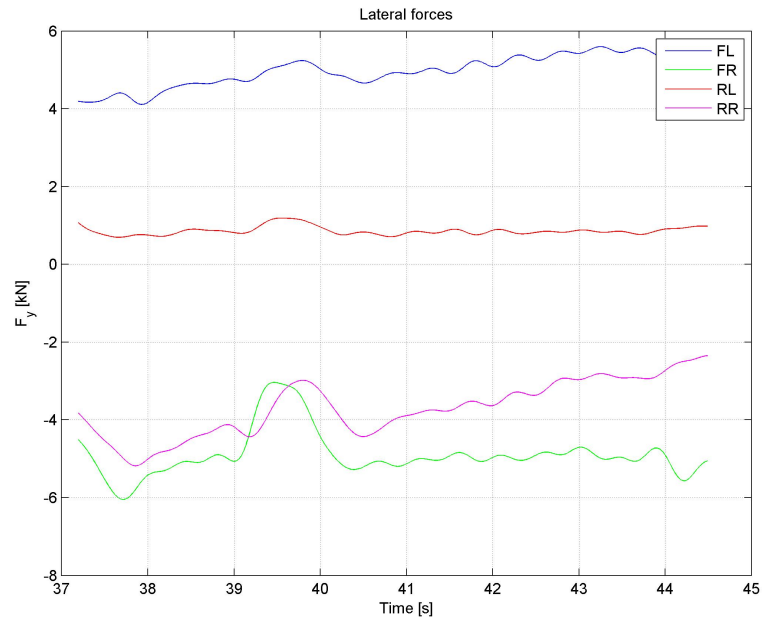


Figure 4.31: Lateral forces during non-linear vehicle maneuver

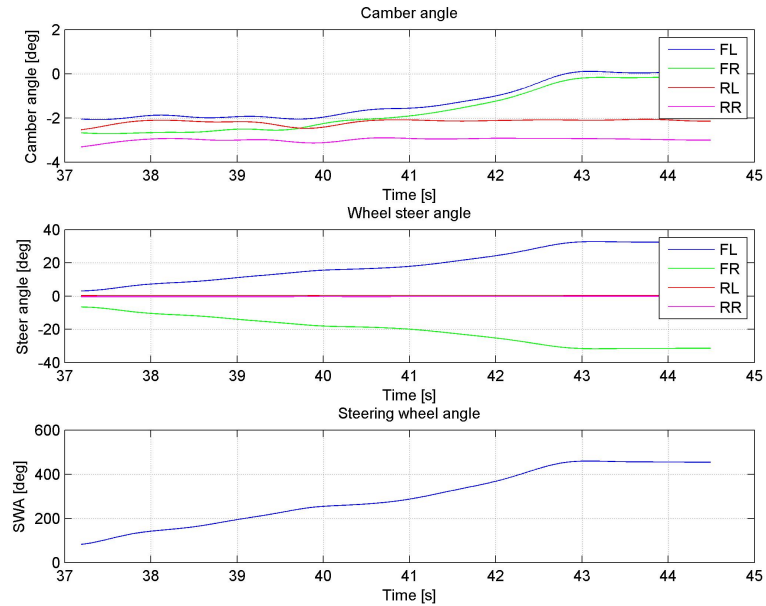


Figure 4.32: Wheel angles during non-linear vehicle maneuver

4.6. IN-VEHICLE MEASUREMENTS

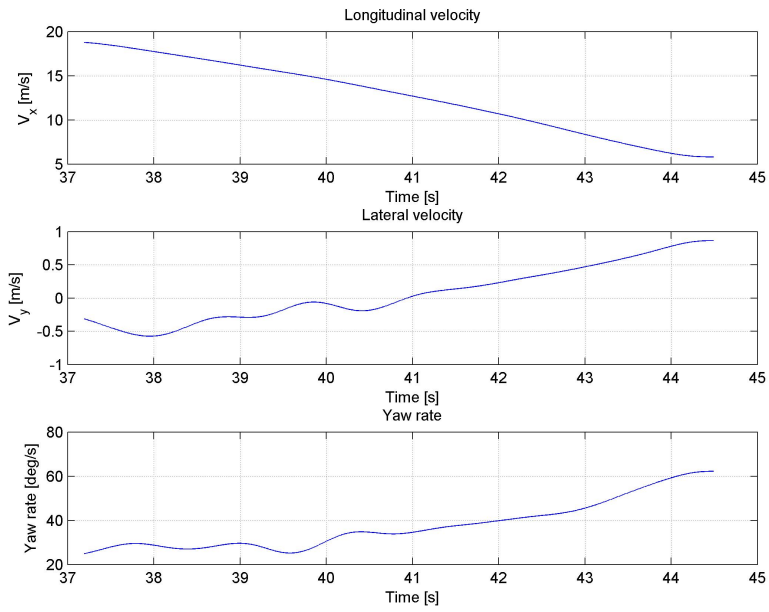


Figure 4.33: Vehicle velocities during non-linear vehicle maneuver

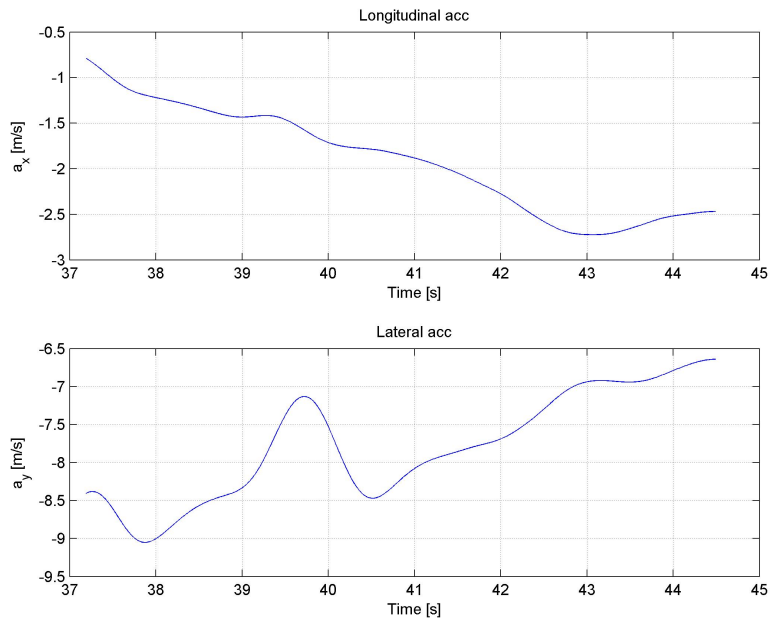


Figure 4.34: Vehicle accelerations during non-linear vehicle maneuver

5

Tire Model Parameter Identification Method

5.1 Post-Processing of Measurement Data

In order to make a full dataset to be used for parameter fitting, first the wheel inclination angles need to be calculated. Since the camera system measures the camber angle relative to the vehicle body and not to the road surface, the roll angle of the vehicle needs to be taken into account in order to know the wheel inclination angle to the road plane. The wheel inclination angle is calculated as shown in equation 5.1.

$$\gamma = \gamma_V + \phi \quad (5.1)$$

Where γ is the inclination angle of the wheel relative to the road plane, γ_V is the wheel camber angle relative to the vehicle, and ϕ is the roll angle of the vehicle relative to the road plane. The roll angle of the vehicle to the road plane is composed of the vehicle roll angle relative to the unsprung mass plus the roll angle due to tire deflection, and can be calculated according to equation 5.2.

$$\phi = \arctan\left(\frac{\Delta WT_{zR} - \Delta WT_{zL} + k_{tire}(\Delta F_{zR} - \Delta F_{zL})}{T}\right) \quad (5.2)$$

Where WT_z is the wheel travel in the Z direction with respect to the vehicle body from static wheel position, k_{tire} is the assumed linear spring rate of the tire, ΔF_z is the change in normal load from static, and T is the track width of the axle. For a perfectly horizontal road, the vehicle roll angle ϕ_V as measured by the IMU will be equal to the roll angle ϕ relative to the road plane. Since the skidpad area is not perfectly horizontal, the roll angles calculated from the wheel travel transducers, camera system, and IMU were compared, and can be seen in Figure A.4 in the appendix.

Since the wheel forces were measured at the wheel hub, it was required to convert the forces into the ISO-W coordinate system to get the forces acting at the tire contact patch. The forces were converted as shown in equation 5.3.

$$\begin{bmatrix} F_{x_w} \\ F_{y_w} \\ F_{z_w} \end{bmatrix} = R \begin{bmatrix} F_{x_c} \\ F_{y_c} \\ F_{z_c} \end{bmatrix} \quad (5.3)$$

Where the rotational matrix R is:

$$R = \begin{bmatrix} 1 & 0 & 0 \\ 0 & \cos(\gamma) & \sin(\gamma) \\ 0 & -\sin(\gamma) & \cos(\gamma) \end{bmatrix} \quad (5.4)$$

Since the wheel axis systems are different on the left and right sides of the vehicle, in order to use the dataset in the fitting tool it was also required that all forces, moments, slip angles, and inclination angles were converted into a single wheel axis system. It was therefore chosen to use the left side axis system as the standard for the fitting tool. The values for α , F_y , and M_z for the wheels on the right side of the vehicle were mirrored to complete the dataset for the fitting tool.

The complete signal processing scheme from measurement data to fitting tool is shown in Figure 5.1 below.

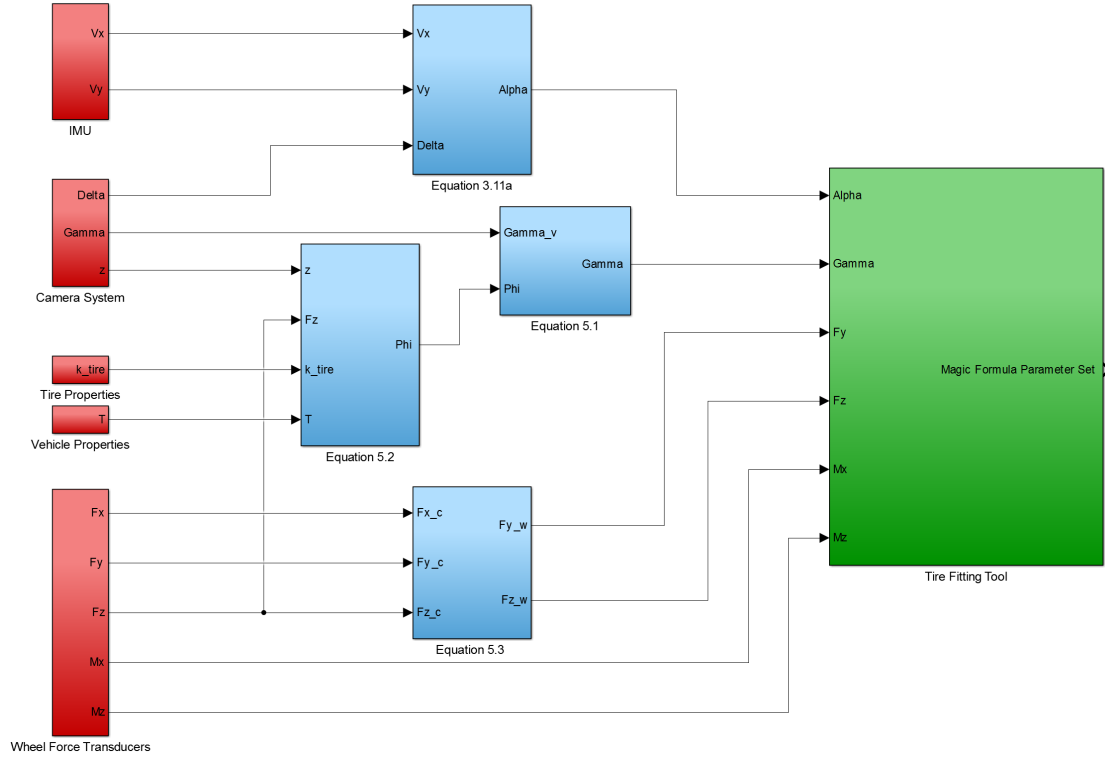


Figure 5.1: Measurement signal processing for use as input to the Magic Formula

5.2 Method

In order to identify the Magic Formula parameters from a dataset, a fitting tool was created using Matlab. The fitting tool uses stochastic optimization techniques to minimize the least squares error between the dataset and the fitted tire model. The least squares were used instead of a maximum-likelihood function since the distribution of data was not known. Initially the solver was tested using a traditional gradient descent method, but this proved to only capture local minima of the objective function because of the amount of parameters. The objective function is given by equation 5.5.

$$\min \quad RMS = \sqrt{\frac{\sum_{i=1}^n (F_m[i] - F(\alpha_m[i], \gamma_m[i], F_{z_m}[i]))^2}{n}} \quad (5.5)$$

Where F_m is the measured lateral force, α_m is the measured slip angle, γ_m is the measured inclination angle, F_{z_m} is the measured normal force, F is the modeled lateral force, and n is the number of data points. The optimization algorithm used is Matlab's implementation of a genetic algorithm. This uses the Augmented Lagrangian Genetic Algorithm to solve optimization problems with non-linear constraints (Section 5.6). This algorithm solves the optimization problem with respect to linear constraints, non-linear

constraints, and bounds.

Because of the uneven distribution of data points with respect to slip angle, slip ratio, camber angle, and normal load, an option to normalize and/or weight the data was added to the fitting tool. The data can then be weighted based on slip angle, camber angle, or normal load, depending on whether increased accuracy in certain regions is required of the tire model. The weighting factor w is applied to the RMS error from equation 5.5, and the new objective function becomes equation 5.6.

$$\min \quad RMS = w_i(\alpha_m[i], \gamma_m[i], F_{z_m}[i]) * \sqrt{\frac{\sum_{i=1}^n (F_m[i] - F(\alpha_m[i], \gamma_m[i], F_{z_m}[i]))^2}{n}} \quad (5.6)$$

From the in-vehicle measurements, more data is collected at small slip angles within the linear region of the tire than at high slip angles. Therefore, this area of the tire will have more of an influence on the solver simply because of the greater amount of data points in this region. If the data is normalized based on slip angle then high slip angle data points will have the same importance as smaller slip angles. For example, if a tire model needs to be created for simulations that require more accuracy in the cornering stiffness rather than the peak behavior of the tire it would be beneficial to use a weighting function that favors the linear region of the tire. An example of such a weighting function is shown in Figure 5.2. However, for the purposes of this thesis the data was not normalized or weighted.

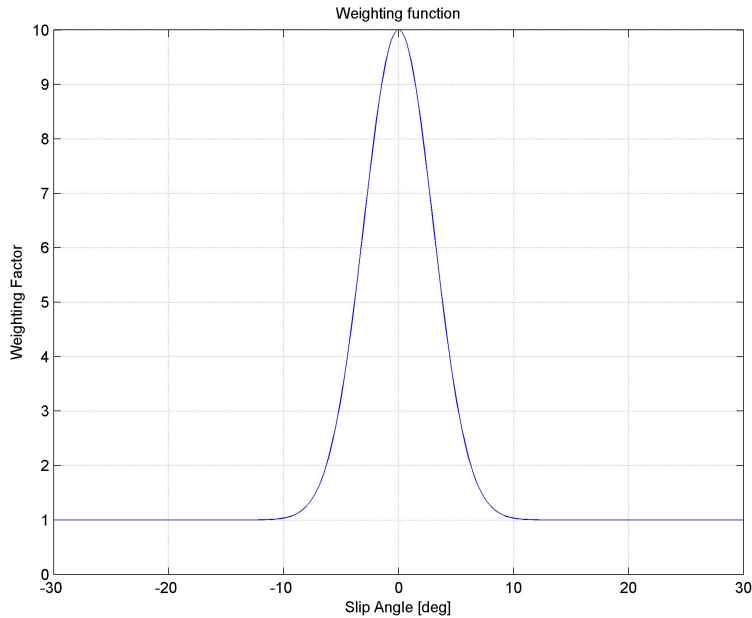


Figure 5.2: Example weighting function that can be applied during fitting process.

5.3 Fitting Requirements

Since the nature of the Magic Formula is that there is dependence between the calculated outputs, the parameter fitting for each case must be done in a specific order. For instance, fitting of the pure slip lateral parameters must be completed before fitting of the overturning moment or aligning moment can be completed. The prerequisites required for fitting are shown in Table 5.1.

Parameter to fit:	Prerequisites:
Pure F_y	None
Pure M_x	Pure F_y
Pure M_z	Pure F_y
Pure M_y	Pure F_x

Table 5.1: Prerequisites for parameter fitting. (MSC Software, 2013 [1])

5.4 Non-Linear Constraints

Non-linear constraints were set according to the PAC2002 tire model standard to prevent unrealistic tire model behavior, as shown in Table 5.2.

$C_y > 0$
$D_y > 0$
$E_y \leq 1$
$pD_{y1}/pD_{y2} < 0$
$K_y < 0$

Table 5.2: PAC2002 constraints. (MSC Software, 2013 [1])

5.5 Parameter Bounds

Each Magic Formula parameter is also given an upper and lower bound in order to provide the solver a realistic range for the parameters. These bounds have been manually set after analyzing over 100 different tire property files available at Volvo Cars. While these boundary conditions work well for passenger car tires, modifications to the bounds may be necessary for other tire constructions. If any of the Magic Formula parameters approach a boundary condition during the fitting process, a warning is generated to allow the boundary conditions to be modified before running the fitting process again.

5.6 Genetic Algorithm

Initial testing of the optimization problem with a gradient decent based solver to identify the four basic parameters (B , C , D , and E) provided solutions with very good fit to the input data. However, the full Magic Formula equation requires the optimization to identify 18 parameters for lateral force, 25 parameters for aligning moment, and 3 parameters for overturning moment. Attempts at using a gradient decent based solver were only able to produce local minima with poor fits to the input data. For this reason it was chosen to use a global optimization solver. The Augmented Lagrangian Genetic Algorithm was chosen after it was shown to produce excellent parameter set results from Flat-Trac datasets, as can be seen in Section 5.7. This solver first begins with a random initial population of individuals (set of parameter guesses) and evaluates the objective function. Then the individuals of the population are scored based on their fitness values. Some of the individuals with the best fitness values are passed on to the next generation. The other individuals become parents, and produce children either by randomly modifying their values, or by combining their values with another individual. This repeats until the change in the fitness value from one generation to the next is less than the defined convergence limit (Whitley, 1995 [6]). This method is slower than the gradient decent method, but produces excellent results.

5.7 Validation of Fitting Tool

The fitting tool has been validated by fitting Flat-Trac measurement datasets and comparing the results to the tire property files provided by the manufacturer with the raw data. In all cases the fitting tool produced tire property files that do not violate any of the constraints established by the PAC2002 standard. In contrast, several of the tire property files provided by tire manufacturers and tire research facilities violate constraints that result in unrealistic tire behavior occurring in isolated regions of the model.

The tire that was chosen for testing was the Michelin Primacy HP 225/50R17, as fitted on a 17x7.5J wheel. Flat track datasets and tire property files have been provided by Michelin for three different inflation pressures. The fitting tool was run on the three Flat-Trac datasets in order to verify the ability to accurately reproduce a tire property file. The RMS values of the fitted tire model to the raw data have been compared to the RMS values of the manufacturer provided tire model, and can be seen in Table 5.3.

5.7. VALIDATION OF FITTING TOOL

Tire source	RMS Error		
	F_y [N]	M_x [Nm]	M_z [Nm]
Michelin provided (180kPa)	244.04	69.20	21.18
Michelin provided (260kPa)	232.69	88.86	14.53
Michelin provided (340kPa)	259.01	102.22	12.92
Fitting tool result (180kPa)	208.56	22.68	15.35
Fitting tool result (260kPa)	203.95	21.57	12.46
Fitting tool result (340kPa)	226.22	20.65	6.91

Table 5.3: Comparison of RMS values between tire property files provided by manufacturer and files created by fitting tool

As can be seen in Table 5.3, the fitting tool developed for this research produces tire property files that exceed the accuracy of the tire property files provided by the tire manufacturer. Furthermore, since the tire property files do not violate any of the PAC2002 constraints, these models tend to be valid over a greater range of the independent variables. The lateral force versus slip angle for the fitted parameters and the Michelin provided parameters can be seen in Figure 5.3.

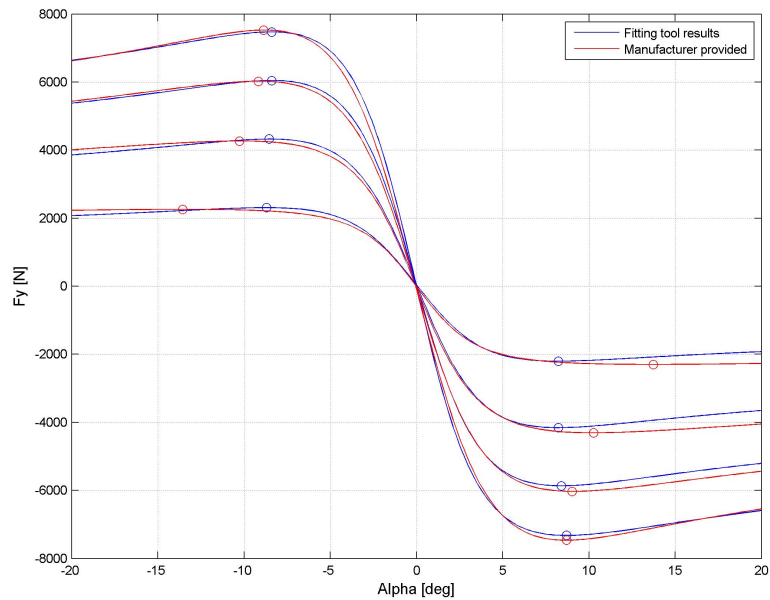


Figure 5.3: Lateral force vs. slip angle showing results from parameter fitting Flat-Trac data compared to Michelin provided tire file for 4 different normal loads

5.7. VALIDATION OF FITTING TOOL

As can be seen above, the results are very close to the Michelin provided tire property file. The cornering stiffness for normal loads from 0 to 16000N is shown in Figure 5.4.

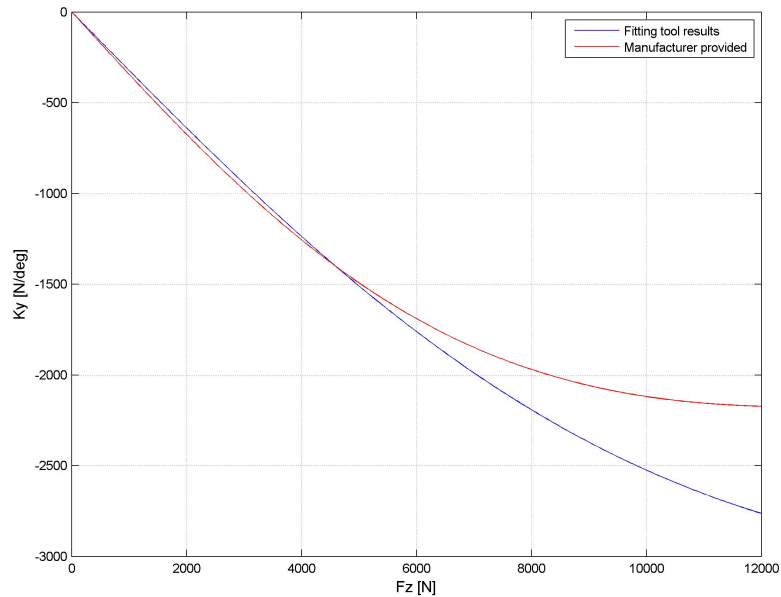


Figure 5.4: Cornering stiffness vs. normal load showing results from parameter fitting Flat-Trac data compared to Michelin provided tire file.

The cornering stiffness of the fitting results matches closely with the Michelin provided tire property file from 0N to approximately 5000N, but after this there are large differences between the Michelin provided tire file and the fitting results. The maximum normal loads from the Flat-Trac dataset are around 8500N, so the fact that there are differences in the cornering stiffness below this force shows that one of the parameter sets is misestimating the cornering stiffness. The friction coefficient versus normal load can be seen in Figure 5.5 below, which has a good correlation to the Michelin provided parameters.

5.7. VALIDATION OF FITTING TOOL

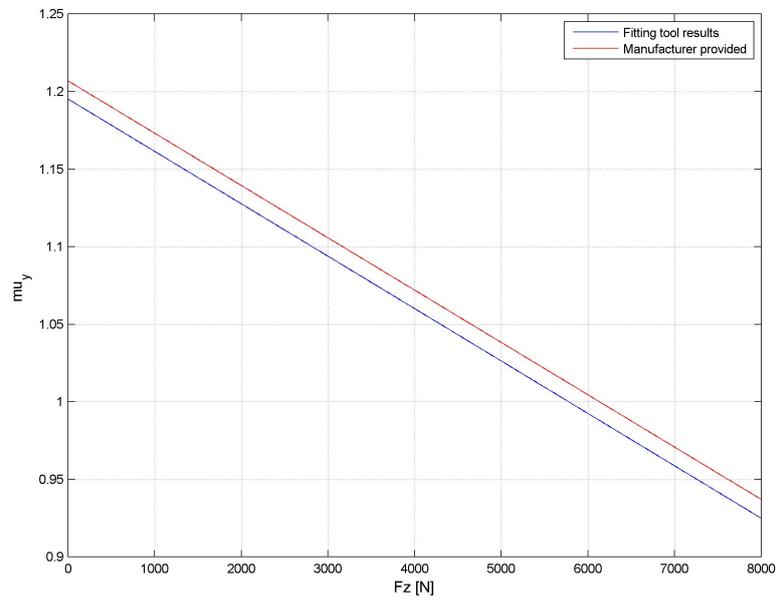


Figure 5.5: Friction coefficient vs. normal load showing results from parameter fitting Flat-Trac data compared to Michelin provided tire file.

6

Identification of Magic Formula Tire Model Parameters

6.1 From Lateral Force with Gaussian Noise

To test the functionality of the fitting tool, values for lateral force were calculated from an existing PAC2002 tire property file with inputs of slip angles, camber angles, and normal loads. The slip angles, camber angles, and normal loads were generated as a normally distributed data set around a given average value. Noise was then added to the calculated lateral force data points to simulate variance in the measurement data, given by equation 6.1. The noise was normally distributed White Gaussian noise with a variance σ^2 .

$$F'_y = F_y + w, \quad (6.1)$$

$$w \sim N(0, \sigma^2) \quad (6.2)$$

where

F_y Lateral force as calculated from the PAC2002 tire file

F'_y Lateral force with added noise

w Normally distributed noise

σ Standard deviation of noise

The sensitivity to the amount of data points was investigated, and it was determined that there is a marked increase in the accuracy of the fitted tire model when more data points are used. The RMS values of the fitted result to the original data and data with noise added can be seen in Table 6.1.

Data Points:	RMS to F'_y [N]	RMS to F_y [N]
1000	535	157
4000	497	49

Table 6.1: RMS values of fitting tool result

The difference in the RMS error to the input data (lateral force with added noise) was only 38N lower (about 7%) when 4000 data points were used compared to 1000 data points. However, the difference is much greater when comparing the result to the original lateral force data before noise was added, having less than one third of the RMS error between 4000 and 1000 data points.

6.2 From Simulation Data

After the fitting tool was verified to fit parameters from the randomly generated data, a dataset from the VI-CarRealTime simulations was created. The lateral force versus slip angle of the combined dataset containing both the linear and non-linear maneuvers is shown in Figure 6.1.

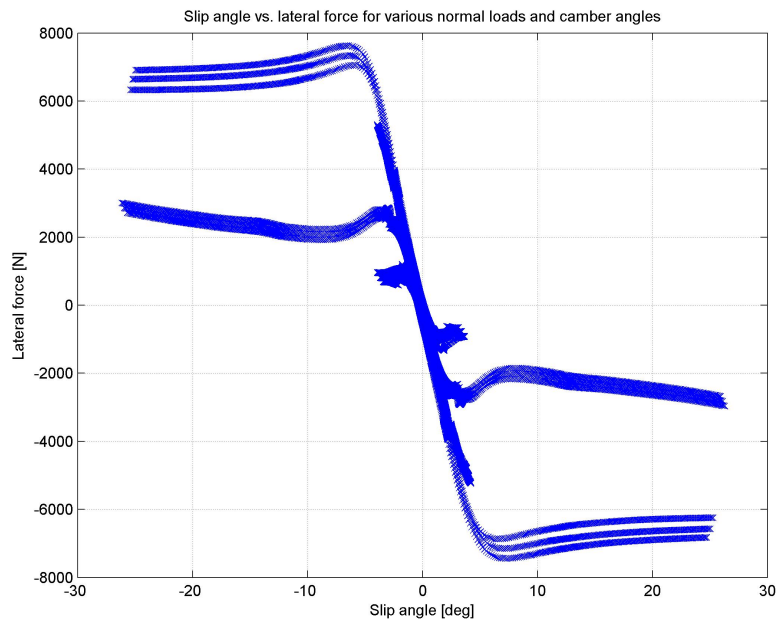


Figure 6.1: Lateral force vs. slip angle of VI-CarRealTime simulations

The results from fitting the simulation dataset can be seen in Figures 6.2 and 6.3 compared to the tire property file as used in the simulations. The circles on the graphs show

6.2. FROM SIMULATION DATA

the peak lateral force or aligning moment achieved by the tire for each of the normal loads. As can be seen, not only does the fitted tire model provide an excellent fit for the cornering stiffness and limit behavior of the tire, it also accurately fits the peaks.

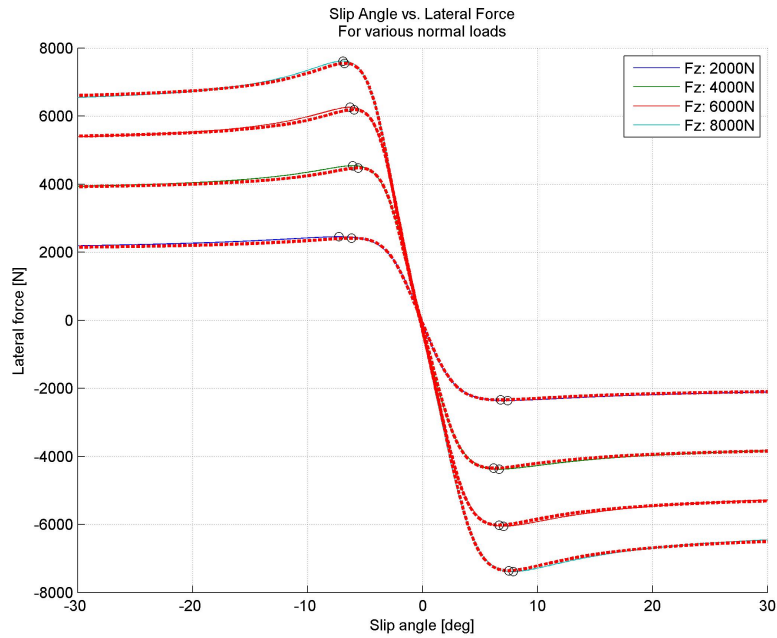


Figure 6.2: Lateral force versus slip angle of fitting tool result compared to original tire property file (dashed red lines)

6.3. FROM MEASUREMENT DATA

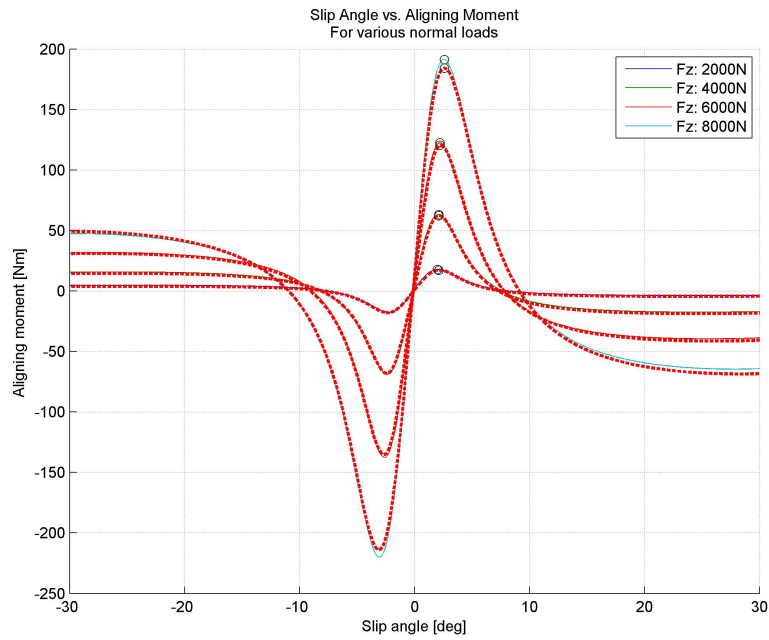


Figure 6.3: Aligning moment versus slip angle of fitting tool result compared to original tire property file (dashed red lines)

6.3 From Measurement Data

The complete dataset made up of the linear and non-linear tests can be seen in Figure 6.4. This figure shows the measurement data as collected in the left side wheel coordinate system.

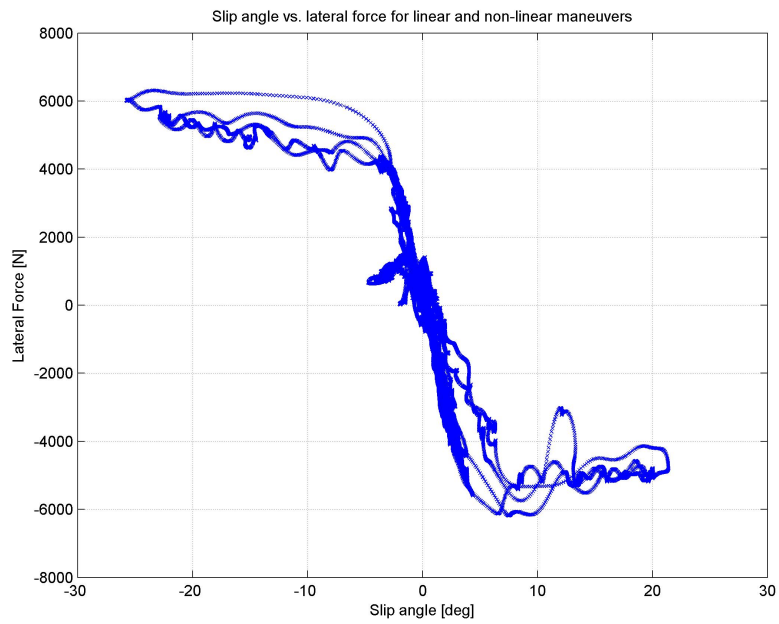


Figure 6.4: Complete dataset composed of linear and non-linear measurements

Results from running the fitting tool on the dataset created from the in-vehicle measurements show that the tire is accurately represented in the areas where data was available. Lateral force versus slip angle for the fitted tire compared to the tire model supplied by the manufacturer from Flat-Trac measurements can be seen in Figure 6.5.

6.3. FROM MEASUREMENT DATA

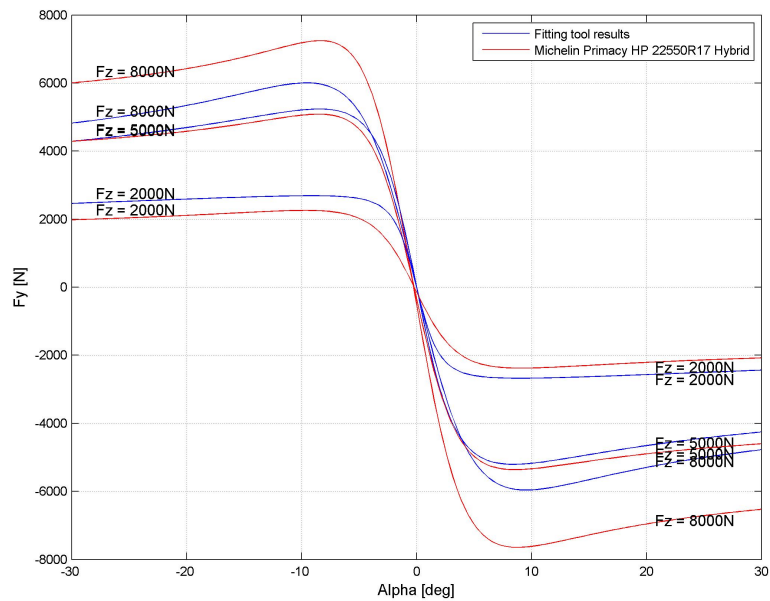


Figure 6.5: Lateral force versus slip angle for fitted tire model (blue) and Flat-Trac tire model from manufacturer (red)

As can be seen, the fitted tire matches closely to the manufacturer's tire model in the areas where data is available, both in the cornering stiffness and peak behavior. The lateral force versus slip angle for normal loads of 4000N and 6000N can be seen in Figures 6.6 and 6.7, respectively. However, in the region where the tire sidewall began oscillating during the testing maneuvers, the manufacturer's tire model overestimates the lateral force the tire provides, as shown in Figure 6.8.

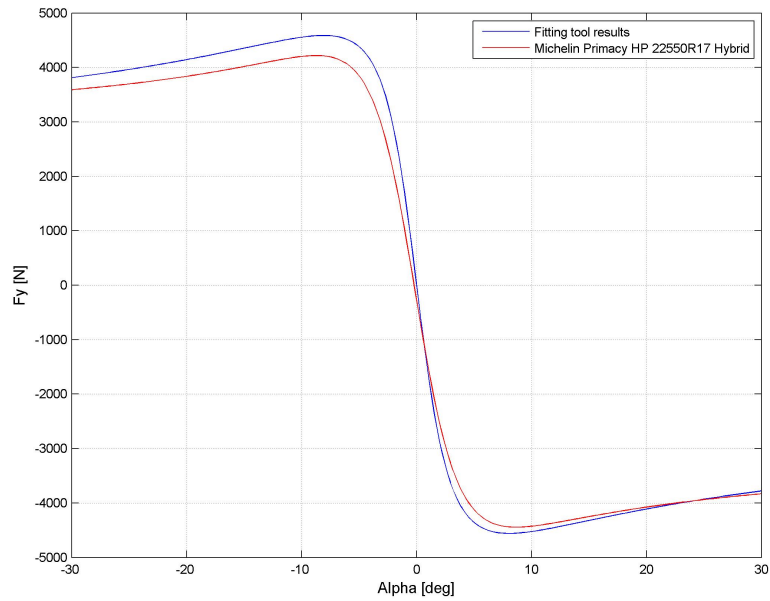


Figure 6.6: Lateral force versus slip angle for fitted tire model (blue) and Flat-Trac tire model from manufacturer (red), $F_z = 4000\text{N}$

In Figure 6.6 above it can be seen that the correlation of the fitted tire model to the manufacturer provided tire file is much better for positive slip angles than for negative slip angles. This is because most of the data that was collected for normal loads of around 4000N was from the inside front wheel, where positive slip angles occurred. Conversely, Figure 6.7 shows a much better correlation for negative slip angles, because the data collected for normal loads around 6000N were mostly from the outside front wheel, which had negative slip angles.

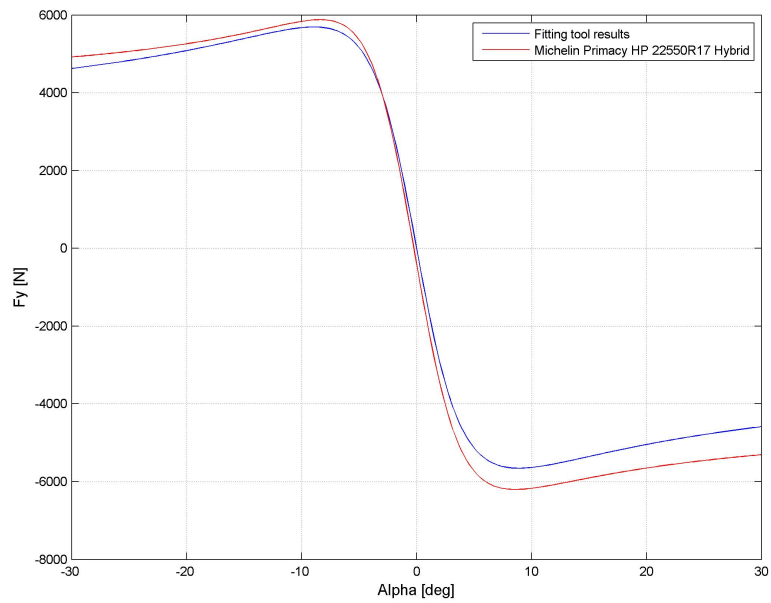


Figure 6.7: Lateral force versus slip angle for fitted tire model (blue) and Flat-Trac tire model from manufacturer (red), $F_z = 6000\text{N}$

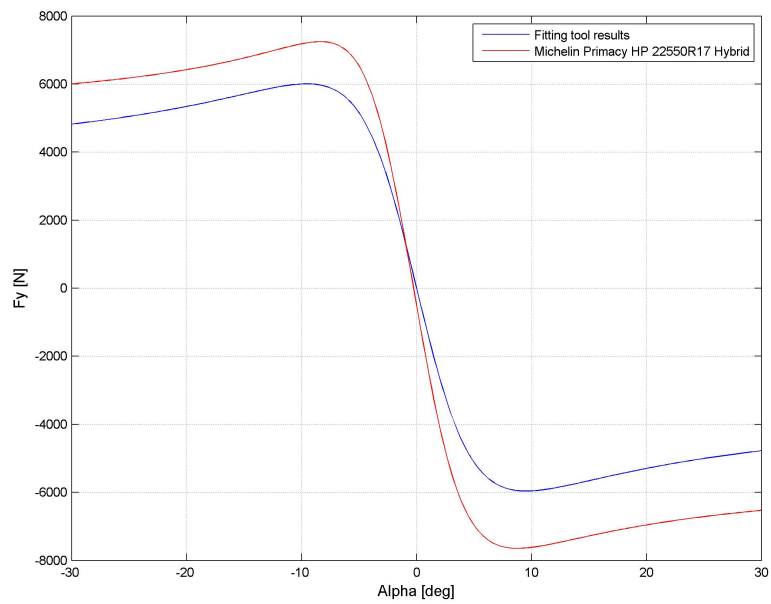


Figure 6.8: Lateral force versus slip angle for fitted tire model (blue) and Flat-Trac tire model from manufacturer (red), $F_z = 8000\text{N}$

Figure 6.8 shows much less correlation to the manufacturer's tire file for two reasons. First, normal loads of 8000N are not encountered on the inside wheels, so no data exists in the dataset for positive slip angles with this normal load. Secondly, since the tire sidewall started oscillating in the tests that were performed, the lateral force of the tire stopped increasing with increasing normal load after reaching a normal load of around 6000N. This outlines one of the major limitations from creating tire model parameters using this method. Further investigations show that it is difficult to capture the cornering stiffness at normal loads that no data is present in, as well as the areas where the tire sidewall is oscillating, as shown in Figure 6.9.

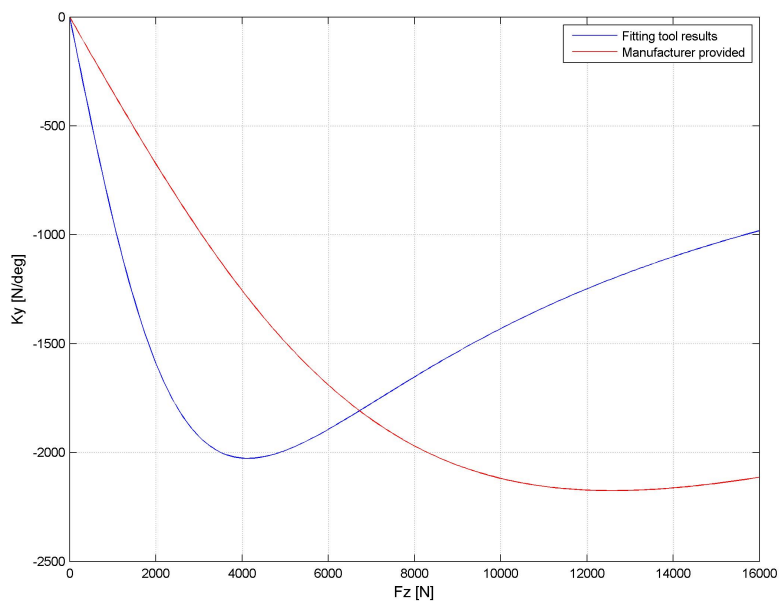


Figure 6.9: Cornering stiffness versus normal load for fitted tire model (blue) and Flat-Trac tire model from manufacturer (red)

As can be seen, the fitting results from in-vehicle measurements overestimate the cornering stiffness at low normal loads, which then decreases sharply above 4000N with a behavior that does not match the tire property file provided by the manufacturer. This is largely due to the effect of the tire sidewall oscillating and losing grip at high normal loads. Similarly, the friction coefficient versus normal load is shown in Figure 6.10.

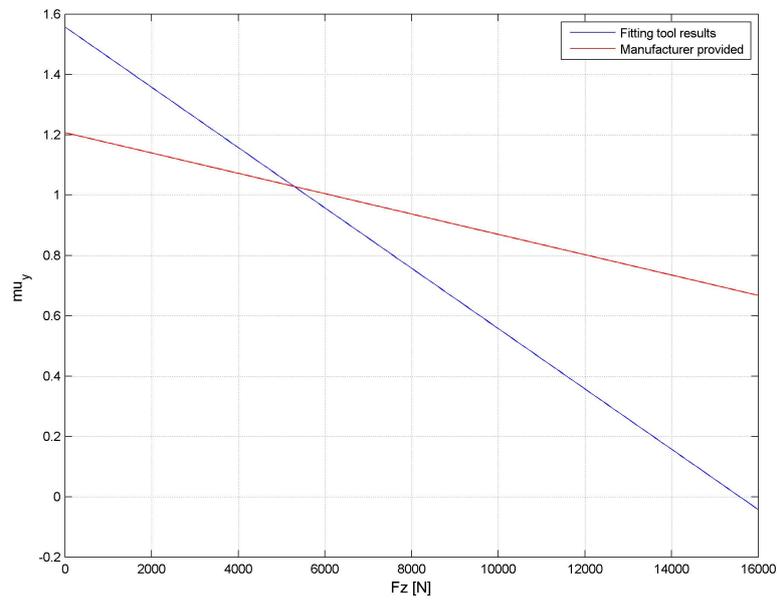


Figure 6.10: Peak friction coefficient versus normal load for fitted tire model (blue) and Flat-Trac tire model from manufacturer (red)

Again, at higher normal loads the results from in-vehicle measurements are much lower than the manufacturer provided tire property file. Another way to see this is by comparing lateral force to normal load, as shown in

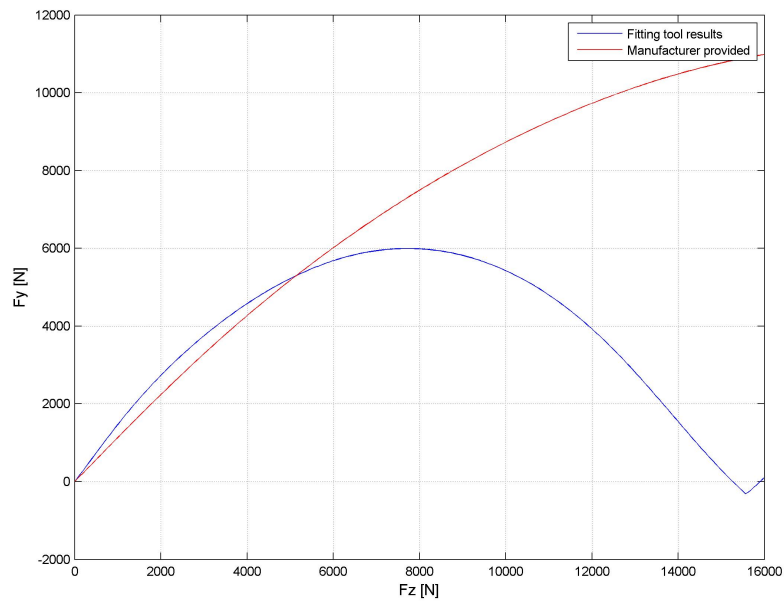


Figure 6.11: Lateral force versus normal load at -10 degree slip angle for fitted tire model (blue) and Flat-Trac tire model from manufacturer (red)

As can be seen above in Figure 6.11, for an example slip angle in the non-linear region of the tire of -10 degrees, the fitting results of the in-vehicle measurements shows a large discrepancy to the manufacturer provided tire file. This shows that above a normal load of around 8000N, no more lateral force can be generated by this tire. This is a very low peak for a production car tire, and has more to do with the tire sidewall oscillations than with the actual tire behavior.

7

Discussion

7.1 Testing procedure

7.1.1 Maneuvers

The testing procedures used where all data is collected on a skidpad circle has some obvious advantages. It allows quick, repeatable gathering of data for a large range of slip angles and normal loads. The nature of the maneuvers also reduces the influence of tire transient effects to a minimum. A drawback with this kind of testing is that the high amount of energy fed into the tires, at a relatively low speed, leads to a rapid temperature increase. A controlled method for data collection is therefore required for repeatability. An alternative method could be to acquire the linear range data from driving at a slow pace (up to approximately 0.5 g cornering) on a handling track, or similar. This would give data that more closely resembles the tire temperatures achieved in normal driving conditions, but could also add hysteresis and transient effects to the data.

7.2 Magic Formula Parameter Fitting Method

When parameterizing the Magic Formula a genetic algorithm was used that aims to find the global minimum of the objective function within the boundaries given. A weighting function that can increase the importance of different input variable ranges was also incorporated. By using a weighting function the importance of the cornering stiffness could be emphasized, for example. Considering that the distribution of data points in the slip angle range was not uniform nor ideal, this could possibly lead to more accurate results.

Another method would be to select the slip angle range around 0, say between -1 and 1 degrees, for all camber angles and normal loads. This subset of data can then be used to parameterize the cornering stiffness equation 3.9. In the same fashion the data that

corresponds to the highest friction coefficient could be selected, and used to parameterize the friction coefficient equation. These parameterizations could easily be done with a fast gradient-based optimization algorithm. The converging values could then be set as fixed boundaries in the global optimization. The effect of this would be that the most important behaviors for passenger car tires, cornering stiffness and maximum friction coefficient, would be emphasized in the parameterization from the beginning, without the potential negative effects of weighting. It would also help to speed up the solution, since fewer parameters would have to be parameterized with the global optimization algorithm.

7.3 Tire Phenomena

As can be seen in Figures 7.1 and 7.2, when the tire that was used for testing becomes saturated and has a high normal load, the sidewall starts oscillating laterally. This can also be seen in Figure 7.3 of the unfiltered measurement data for the front right tire in lateral and normal forces.



Figure 7.1: Tire marks on asphalt

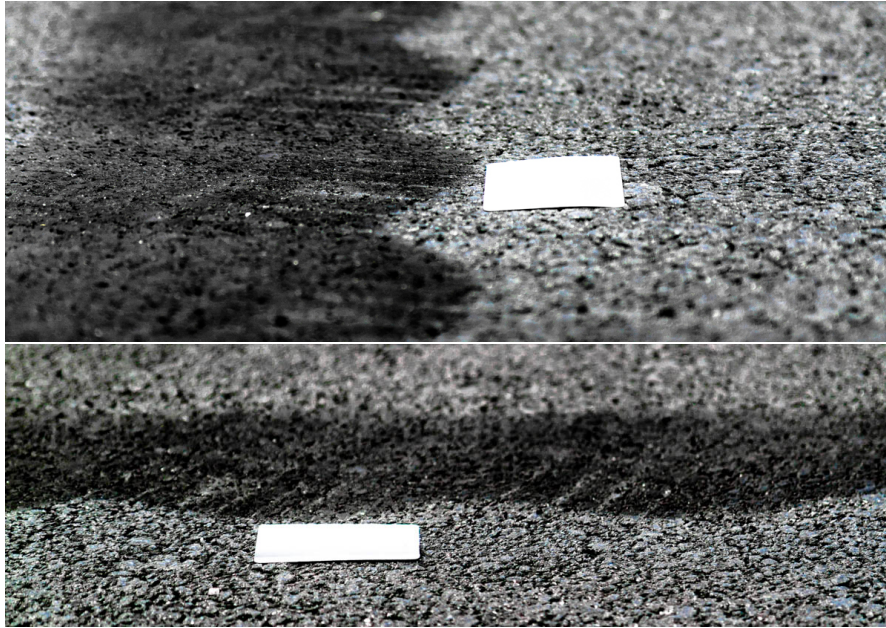


Figure 7.2: Tire marks on asphalt, 86mm x 54mm card for scale

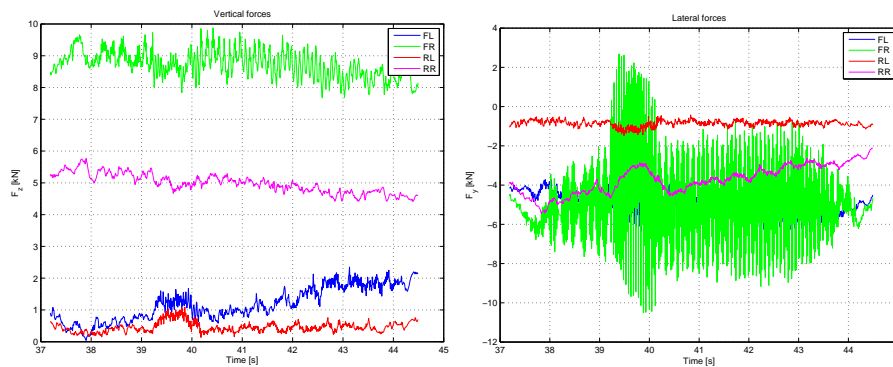


Figure 7.3: Oscillating measurement data for normal and lateral force on the front right tire (green) during the non-linear maneuver because of tire sidewall oscillation.

When the tire sidewall starts oscillating in this way, since the PAC2002 tire model is not a physical tire model it can only capture the average force behavior of the tire. What was observed during the sidewall oscillation was that the tire stopped providing an increase in lateral force with an increase in normal force. This was the result that we were able to achieve, as it was not able to reach the lateral force levels on the vehicle that were expected based on the manufacturer provided tire property file.

Since the results from fitting the in-vehicle measurements represent characteristic behavior of this specific vehicle while at the same time have large differences to the man-

ufacturer provided tire property file, it is clear that other factors are influencing the results. The tire sidewall oscillations that limit the range of data that could be collected could possibly have been caused by stick-slip effects from the front strut assemblies. By replacing the original front spring with a smaller diameter racing spring to ensure clearance for camber adjustments, some unwanted effects were introduced. The side-force on the damper was increased without the compensation from the original spring that was offset on the strut. This creates more friction in the damper, which in turn creates stick-slip effects that are a possibly cause for the variance in force measurement data. To prevent this, a side-force compensated spring should be used for these tests. This was not achievable given the physical limitations of the vehicle if camber sensitivity was to be considered. For a more robust measurement solution a vehicle with large wheel clearance to accommodate several camber angles, as well as side-force compensated springs should be used.

7.4 Limitations

Several limitations were found when using this procedure to produce tire model parameters. Firstly, the normal loads that exist on each of the four tires are fixed based on the vehicle's center of gravity location, lateral acceleration, and roll stiffness distribution. This makes it difficult to collect data for high slip angles with low normal loads, and low slip angles with high normal loads. Along with this, the kinetics of the vehicle suspension provide an increase in positive camber angle with load transfer and roll, so even by using a static camber angle of -3 degrees, the inclination of the outside wheels to the ground at maximum lateral acceleration is around 0 degrees. Because of this there is a lack of data for negative camber angles with high normal loads and high slip angles.

These limitations can mostly be addressed by compensating with exaggerated static camber and toe angles in order to collect data in the necessary regions, but this requires more test maneuvers to be run. To increase the range of normal loads that can be used, ballast can be added to the vehicle. However, this can mostly only be used to collect data for increased normal loads. The data of real interest that is missing from this method is normal loads near the static normal loading of the tires with high slip angles. In order to achieve this, ballast would need to be added with a lateral offset in order to reduce the normal load on the outside tires during maximum lateral acceleration.

Apart from the above limitations, since this method requires testing with an actual vehicle on a real road surface, it takes much more time to complete than testing in a lab environment. There are also more outside factors such as weather and track conditions that affect the repeatability of measurements.

7.5 Advantages

This method of producing tire model parameters has several benefits when compared to standard Flat-Trac measurements. Since the measurements are conducted on the vehicle on real asphalt, the tire model that is produced by this method more accurately represents the actual behavior of the tire on the specific surface that was used for the measurements. This also provides an opportunity to conduct the measurements on different surface materials or conditions, such as on wet asphalt or a frozen lake. Because of this it can be valuable to measure tires during different conditions to discover more about the tire behavior than what is shown by lab testing in a Flat-Trac machine. Furthermore, the turnaround time for results with this method is fast, as a fitted tire property file can be created after one day of physical testing.

8

Conclusion

In simulations it has been clearly shown that it is possible to fit a tire very well using data from in-vehicle measurements (Chapter 6.2). The fit correlates almost perfectly to the Magic Formula model used in the simulations. Even with noise added a very good fit is obtained, provided a sufficient amount of data points has been gathered (Table 6.1). Based on this, there is reason to believe that the developed method can be used with successful results.

From the physical in-vehicle measurements, a fitted tire model has been created, but not validated. There were some obstacles during the in-vehicle testing, and ideally it should be redone, with all tests carried out in the same ambient conditions, without interruptions, and with modifications to the vehicle to reduce slip-stick effects. In general the fitting results seem to accurately represent what was measured on the car.

The oscillating behavior that occurred during the measurement is not always as prominent in all cars, and changes widely with tire construction and suspension compliance. It is also a behavior that is mainly triggered after a non-negligible amount of time at high slip angles. It is reasonable to believe (but not validated), that a tire that is parameterized using data that includes oscillating behavior would not represent a dynamic maneuver close to limit handling very accurately, for example a moose test or a step steer input. In a Flat-Trac rig measurement, the input variables (normal load, inclination angle, and slip angle) are easily maintained at controlled levels, therefore unstable tire behavior is not provoked. It is possible that this method is better suited for stiffer, lower profile tires, that are not as prone to unstable behavior. An investigation is needed to understand what causes the instabilities in the tire, and if there are ways to avoid these problems entirely.

For validation of the results, simulations of the vehicle that was used in the measure-

ments, with the parameterized tire model, and the recorded wheel angles and longitudinal velocity profile as input, should be run. Comparisons of acceleration and displacement data will make a good metric for model validity. Initially a simple skidpad test could be valuable, which describes the easiest possible steady state driving case. Other, more demanding driving cases should also be considered, such as sine sweeps or driving on country roads. The driving case needs to minimize the influence of longitudinal dynamics for the highest accuracy.

Overall, a valid method has been created to create tire property files using in-vehicle measurements, but further research should be carried out to reduce errors in the measured input variables to the Magic Formula. Once this is done, with new maneuvers this method can easily be extended to longitudinal force, and eventually combined slip weighting functions can be parameterized.

Bibliography

- [1] MSC Software, Using the PAC2002 Tire Model (2013).
- [2] J. J. M. v. Oosten, C. Savi, M. Augustin, J. Bouhet, J. Sommer, J. P. Colinot, TIME, Tire Measurements Forces and Moments: A New Standard for Steady State Cornering Tyre Testing, 1999.
- [3] H. Pacejka, Tire and Vehicle Dynamics, 3rd Edition, Elsevier, 2012.
- [4] TNO Road-Vehicles Research Institute and Universität Karlsruhe, TYDEX-Format Reference Manual, Release 1.3 (2 1997).
- [5] Vehicle Dynamics Standards Committee, Vehicle Dynamics Terminology: SAE Standard J670, Society of Automotive Engineers International, 2008.
- [6] D. Whitley, Foundations of Genetic Algorithms, Vol. 3, 1995.

A

Appendix

A.1 Notations

Definitions that are used in this report come from SAE J670 [5] and Tire and Vehicle Dynamics [3].

A.1.1 Vehicle Definitions

Ground plane: A horizontal plane in the inertial reference, normal to the gravitational vector.

Road surface: The surface that supports the tire and provides friction to create tire forces in the road plane.

Road plane: A plane representing the road surface within each tire contact patch.

Camber angle: The angle between the vehicle's Z-axis and the wheel plane, about the vehicle's X-axis. The camber angle is positive when the wheel leans outward at the top, and negative when the wheel leans inward at the top.

Roll angle (ϕ): The angle between the road plane and the vehicle's Y-axis, about the vehicle's X-axis.

Vehicle roll angle (ϕ_V): The angle between the ground plane and the vehicle's Y-axis, about the vehicle's X-axis.

A.2 Magic Formula Equations

The magic formula includes a set of scaling factors λ . In all work conducted in this thesis, all scaling factors have been set to constant 1. The ξ parameters are concerning turn slip, and have all been set to constant 1 throughout the thesis, as turn slip has been neglected (Chapter 2.1). In addition to the curve creating variables in the Magic Formula, some extra variables and parameters have been defined in equation A.1. A description of parameters and variables in the model can be seen in table A.1. Only the equations for pure lateral steady state cornering has been included. Equations A.2, A.3 and A.4 describes lateral force, aligning moment and overturning moment respectively.

Table A.1: Variables used in the Magic Formula

g	Acceleration due to gravity
V_c	Magnitude of the velocity of the wheel contact center
$V_{cx,y}$	Components of the velocity of the wheel contact center
$V_{sx,y}$	Componenets of slip velocity V_s
V_r	Wheel rolling speed
V_0	Reference velocity
R_0	Unloaded tire radius
R_e	Effective rolling radius
Ω	Wheel rotational speed
ρ_z	Radial deflection of tire
F_{z0}	Nominal (rated) load of tire
F'_{z0}	Adapted nominal load

Normalized variables

$$F'_{z0} = \lambda_{Fz0} F_{z0} \tag{A.1a}$$

$$df_z = \frac{F_z - F'_{z0}}{F'_{z0}} \tag{A.1b}$$

$$\alpha^* = \tan(\alpha) \operatorname{sgn}(V_{cx}) = -\frac{V_{cy}}{|V_{cx}|} \tag{A.1c}$$

$$\gamma^* = \sin(\gamma) \tag{A.1d}$$

$$\tag{A.1e}$$

Lateral Force (Pure side slip)

$$F_y = D_y \sin [C_y \arctan \{B_y \alpha_y - E_y (B_y \alpha_y - \arctan(B_y \alpha_y))\}] + S_{V_y} \quad (\text{A.2a})$$

$$\alpha_y = \alpha^* + S_{H_y} \quad (\text{A.2b})$$

$$C_y = p_{C_y1} \lambda_{C_y} \quad (\text{A.2c})$$

$$D_y = \mu_y F_z \xi_2 \quad (\text{A.2d})$$

$$\mu_y = \frac{(p_{D_y1} + p_{D_y2} df_z) (1 - p_{D_y3} \gamma^{*2}) \lambda_{\mu_y}}{1 + \lambda_{\mu V} V_s/V_0} \quad (\text{A.2e})$$

$$E_y = (p_{E_y1} + p_{E_y2} df_z) \{1 - (p_{E_y3} + p_{E_y4} \gamma^*) \operatorname{sgn}(\alpha_y)\} \lambda_{E_y} \quad (\text{A.2f})$$

$$K_{y\alpha 0} = p_{K_y1} F'_{z0} \sin [2 \arctan \{F_z/(p_{K_y2} F'_{z0})\}] \lambda_{K_y\alpha} \quad (\text{A.2g})$$

$$K_{y\alpha} = K_{y\alpha 0} (1 - p_{K_y3} \gamma^{*2}) \xi_3 \quad (\text{A.2h})$$

$$B_y = \frac{K_{y\alpha}}{C_y D_y + \epsilon_y} \quad (\text{A.2i})$$

$$S_{H_y} = (p_{H_y1} + p_{H_y2} df_z) \lambda_{H_y} + p_{H_y3} \gamma^* \lambda_{K_y\gamma} \xi_0 + \xi_4 - 1 \quad (\text{A.2j})$$

$$S_{V_y} = F_z \{(p_{V_y1} + p_{V_y2} df_z) \lambda_{V_y} + (p_{V_y3} + p_{V_y4} df_z) \gamma^* \lambda_{K_y\gamma}\} \lambda'_{\mu_y} \xi_2 \quad (\text{A.2k})$$

$$K_{y\gamma 0} = \{p_{H_y3} K_{y\gamma 0} + F_z (p_{V_y3} + p_{V_y4} df_z)\} \lambda_{K_y\gamma} \quad (\text{A.2l})$$

Aligning Moment (Pure side slip)

$$M_{z0} = M'_{z0} + M_{zr0} \quad (\text{A.3a})$$

$$M'_{z0} = -t_0 F_{y0} \quad (\text{A.3b})$$

$$t_0 = D_t \cos [C_t \arctan \{B_t \alpha_t - E_t (B_t \alpha_t - \arctan(B_t \alpha_t))\}] \cos'(\alpha) \quad (\text{A.3c})$$

$$\alpha_t = \alpha^* + S_{Ht} \quad (\text{A.3d})$$

$$S_{Ht} = q_{Hz1} + q_{Hz2} df_z + (q_{Hz3} + q_{Hz4} df_z) \gamma^* \quad (\text{A.3e})$$

$$M_{zr0} = D_r \cos [C_r \arctan (B_r \alpha_r)] \quad (\text{A.3f})$$

$$\alpha_r = \alpha^* + S_{Hf} \quad (\text{A.3g})$$

$$S_{Hf} = S_{Hy} + \frac{S_{Vy}}{K'_{y\alpha}} \quad (\text{A.3h})$$

$$K'_{y\alpha} = K_{y\alpha} + \epsilon_K \quad (\text{A.3i})$$

$$B_t = (q_{Bz1} + q_{Bz2} df_z + q_{Bz3} df_z^2) (1 + q_{Bz4} \gamma^* + q_{Bz5} |\gamma^*|) \frac{\gamma K_{y\alpha}}{\lambda_{\mu y}} \quad (\text{A.3j})$$

$$C_t = q_{Cz1} \quad (\text{A.3k})$$

$$D_{t0} = \frac{F_z R_0}{F'_{z0}} (q_{Dz1} + q_{Dz2} df_z) \lambda_t \operatorname{sgn}(V_{cx}) \quad (\text{A.3l})$$

$$D_t = D_{t0} \left(1 + q_{Dz3} \gamma^* + q_{Dz4} \gamma^{*2}\right) \xi_5 \quad (\text{A.3m})$$

$$E_t = (q_{Ez1} + q_{Ez2} df_z + q_{Ez3} df_z^2) \left[1 + (q_{Ez4} + q_{Ez5} \gamma^*) \frac{2}{\pi} \arctan B_t C_t \alpha_t\right] \quad (\text{A.3n})$$

$$B_r = q_{Bz10} B_y C_y \quad (\text{A.3o})$$

$$C_r = \xi_7 \quad (\text{A.3p})$$

$$D_r = F_z R_0 [(q_{Dz6} + q_{Dz7} df_z) \lambda_{Mr} \xi_2 + (q_{Dz8} + q_{Dz9} df_z) \gamma^* \lambda_{Kz\gamma} \xi_0] \cos' \alpha \lambda_{\mu y} \operatorname{sign}(V_{cx}) + \xi_8 - 1 \quad (\text{A.3q})$$

$$K_{z\alpha 0} = D_{t0} K_{y\alpha 0} \quad (\text{A.3r})$$

$$K_{z\gamma 0} = F_z R_0 (q_{Dz8} + q_{Dz9} df_z) \lambda_{Kz\gamma} - D_{t0} K_{y\gamma 0} \quad (\text{A.3s})$$

Overturning couple (Pure side slip)

$$M_x = F_z R_0 \left(q_{sx1} - q_{sx2} \gamma^* + q_{sx3} \frac{F_y}{F'_{z0}} \right) \lambda_{Mx} \quad (\text{A.4a})$$

Effective rolling radius

$$R_e = R_0 + q_{V1} R_0 \left(\frac{\Omega R_0}{V_0} \right)^2 - \rho_{Fz0} \left[D_{Reff} \arctan (B_{Reff} \rho^d) + F_{Reff} \rho^d \right] \quad (\text{A.5a})$$

$$\rho_{Fz0} = \frac{F_{z0}}{C_z \lambda_{Cz}} \quad (\text{A.5b})$$

The model standard used in this thesis is PAC2002, developed by MSC Software for usage in Adams/Tire ([1]).

A.3 Validation of Measured Data

In order to validate that the measured data was reliable, multiple methods were used to analyze the data. Firstly, the steering wheel angle from the vehicle CAN bus was compared to the front wheel steered angles from the WheelWatch measurement system. Correlation between the two data sources was high, as can be seen in Figure A.1.

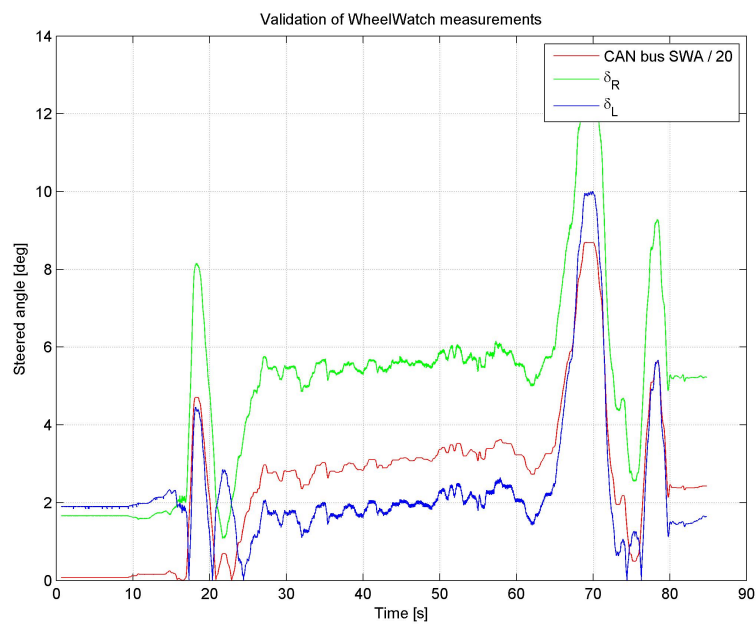


Figure A.1: Vehicle CAN bus SWA signal compared to measured toe angles

In order to validate that the wheel force transducers were providing reliable results, the sum of the lateral forces divided by the mass of the vehicle was compared to the lateral acceleration as measured by the IMU. The correlation between these two sensor systems was good, as seen in Figure A.2.

A.3. VALIDATION OF MEASURED DATA

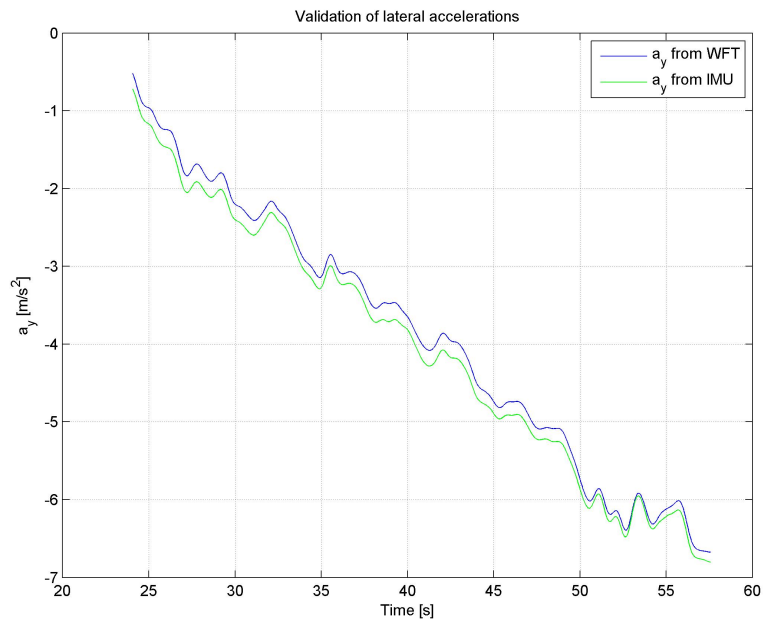


Figure A.2: Sum of WFT lateral forces divided by mass of vehicle compared to IMU lateral acceleration

The sum of the normal loads as measured by the wheel force transducers was also plotted over time for the both the linear and non-linear tests, and are shown in Figure A.3.

A.3. VALIDATION OF MEASURED DATA

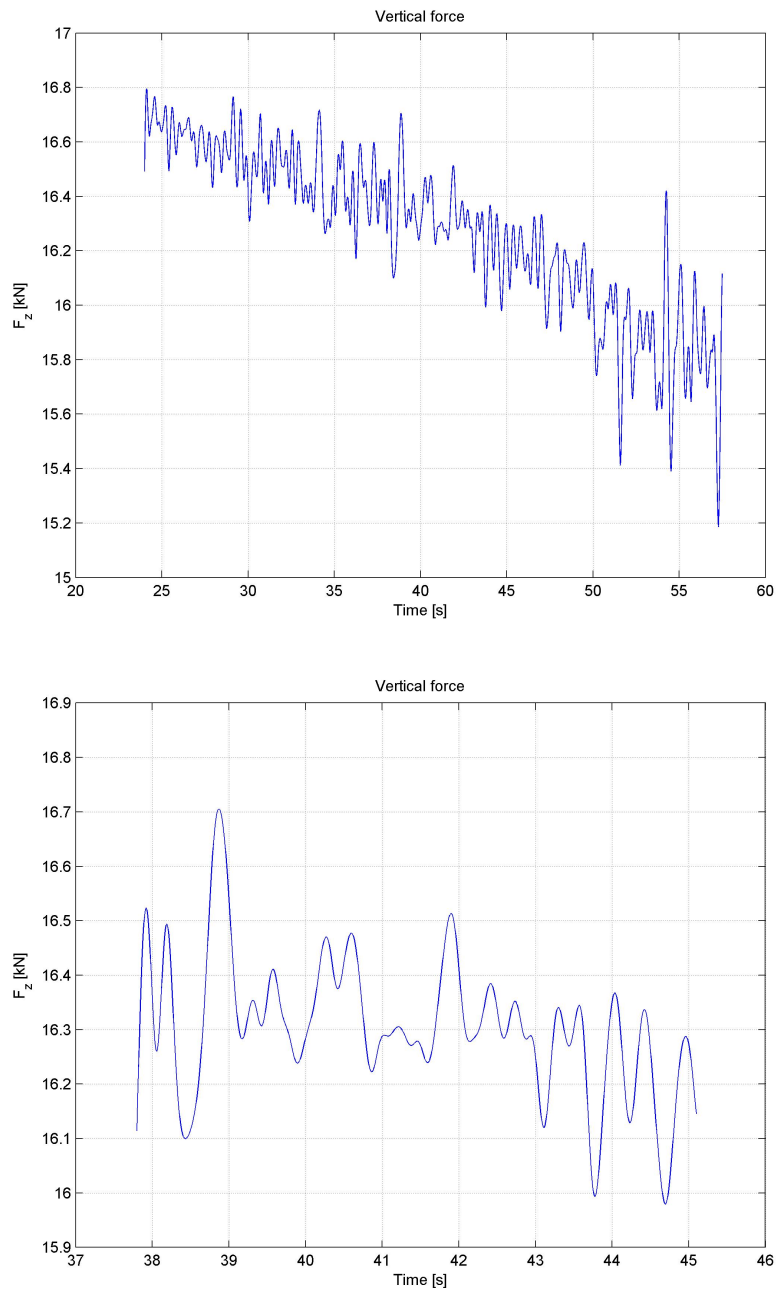


Figure A.3: Sum of WFT vertical forces over time for linear and non-linear maneuvers

Since there is a slight inward grade to the skidpad area where testing was conducted for the measurements, the absolute roll angle value as measured by the IMU would not be accurate for the tire model since what actually is of interest is the roll angle to the road plane. This angle was calculated using the wheel displacements as measured by the

WheelWatch camera system, the normal loads measured by the wheel force transducers, and assuming a linear tire stiffness. The comparison between the calculated roll angle to ground and the absolute roll angle from the IMU can be seen in Figure A.4.

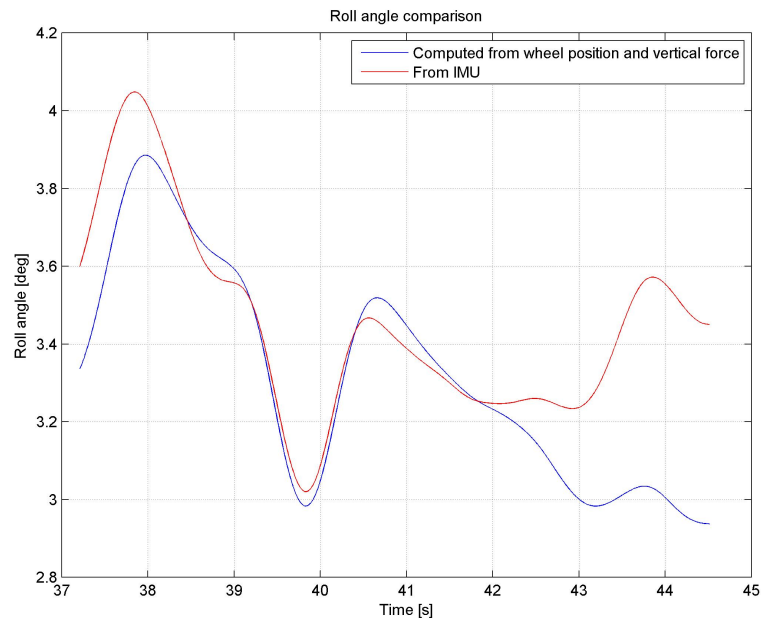


Figure A.4: Vehicle absolute roll angle from IMU compared to vehicle roll angle to surface from WheelWatch system

A.4 Fitting Tool

A.4.1 Graphical User Interface

A graphical user interface was created for the fitting tool in order to more easily load datasets, perform fitting procedures, and view tire files.

A.4. FITTING TOOL



Figure A.5: Main window of tire parameter fitting tool

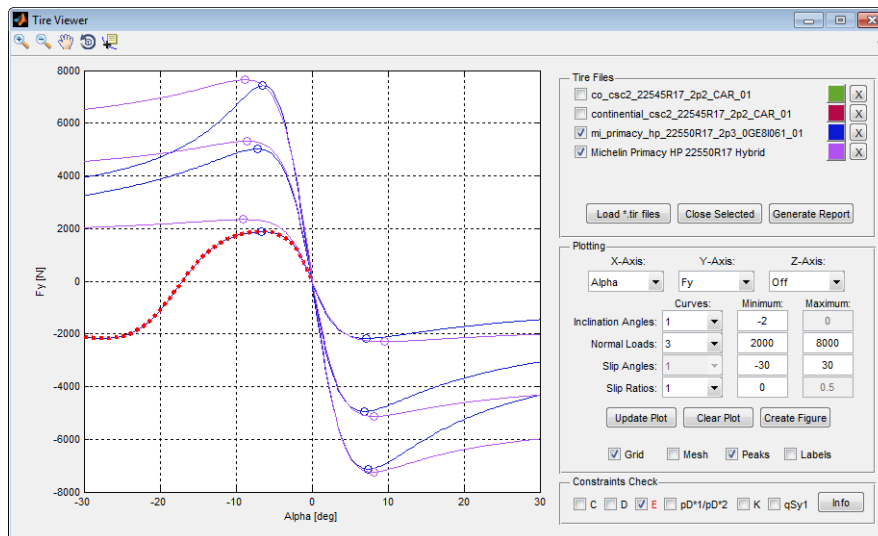


Figure A.6: Tire file graphing utility highlighting area of tire file that does not conform to PAC2002 constraints

A.4. FITTING TOOL

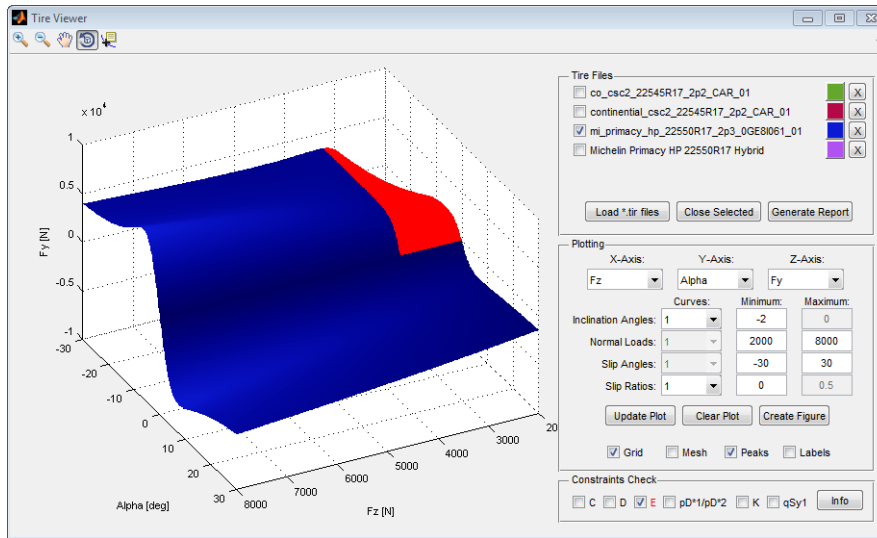


Figure A.7: Tire file graphing utility showing surface graphing ability and area of tire file that does not conform to PAC2002 constraints

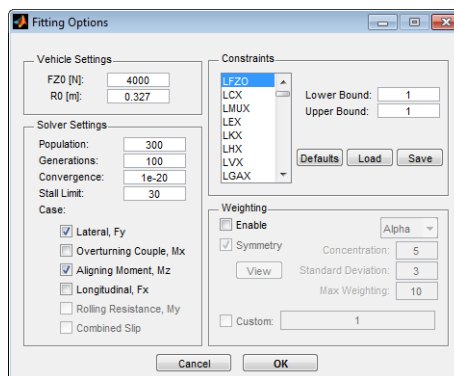


Figure A.8: Options that can be selected while setting up the fitting procedure

A.4. FITTING TOOL

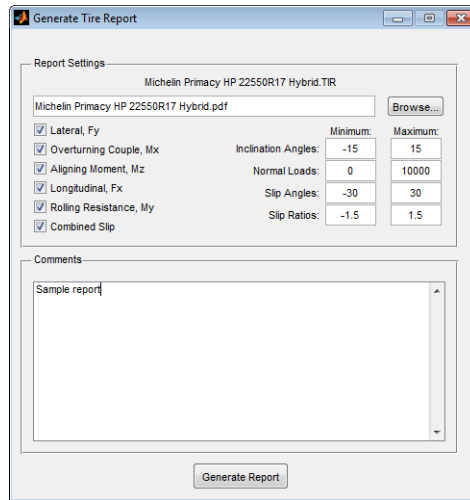


Figure A.9: PDF report generation tool to create a report on tire characteristics from a tire property file

